Repairability of lattice structure in a circular economy:

Mechanical response of 3D printed octet-truss lattice structures under quasi-static loading
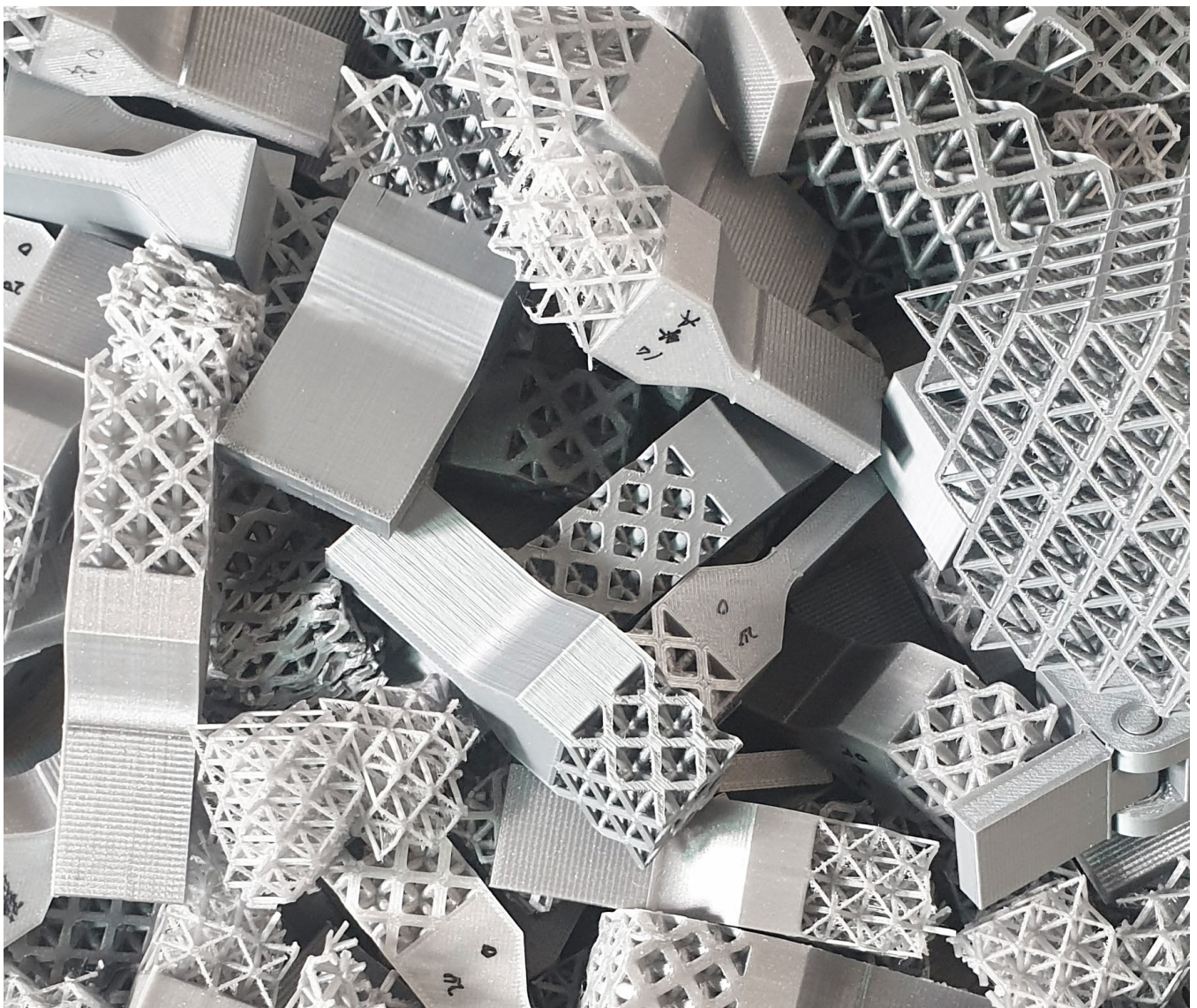
Executive Summaries

Research on the design methodology and production of lattice structures has been widely conducted; however, studies on the repair and maintenance of lattice structures, which play an important role in the circular economies, are rare. In this study, four different tests viz. compressive, tensile, shear, and three-point bending tests were carried out to determine the repairability of the lattice structure and observe the effects of repair in the circular economy.

In each test, the specimens were divided into two groups: standard, which were printed in a single piece, and joined, which were adhesively bonded. These were fabricated using fused deposition modelling (FDM) with polylactic acid (PLA). An octet-truss stretch-dominated lattice, with a strut length of 10 mm and a strut diameter of 1–2.5 mm at 0.5 mm intervals, was used.

The results indicate that the use of compression and shear stress in repair under the constraint of this study can lead to a mechanical response that is most similar to the original state, while tension and flexural stress may lead to failing of the bonded parts before the structure starts yielding. As a result, the direction of stress acting on the product should be considered for the repair of the lattice structure.

Recycling of materials has less impact on the environment and is thus beneficial; however, it is less effective compared to repairing and reusing products as it requires more resources. For the repair of the lattice structure, accuracy is essential because a defective lattice structure may significantly affect the mechanical response of the structure, influencing the functioning. Therefore, accurate repair can play a positive role in extending the life span of a product, thus enabling a more efficient circular economy.

Acknowledgement

Foremost, I would like to express my sincere gratitude to my supervisors, Prof. Balkenende and Dr. Wu, who gave me an opportunity to do my master project in TU Delft. The encouragement and advice you gave me in every meeting enabled me to finish the project more efficiently in a right direction. I would also like to thank them for their empathy, allowed me to keep doing the project in my country under unexpected situation. I was able to finish the project without any problems because they were understanding even in an unusual situation.

"I'm coaching you, not directing you," which I heard in the early days of the project, was a different educational philosophy from what I have experienced in Korea, and reminded me that the reason why I left Korea and studied in TU Delft. The words gave me a sense of responsibility for the project, encouraging me to be actively engaged in the project and improve the level of perfection.

In addition to my committee members, I sincerely thank Ms. Mascha Slingerland, a research engineer, the Faculty of Applied Science, Delft University of Technology. Despite the difficult situation, she continued to help me keep up with the research and allowed me to use the equipment. Without her help, the large amount of tests would not have been completed in time.

Last but not least, I would like to thank my parents who always support me.

Table of contents

Abstract

Repair and maintenance of products require few resources in a circular economy, minimising the environmental impact of manufacturing and use of products. Although lightweight lattice structures have been widely investigated in various fields owing to their advantages in terms of their mechanical characteristics and the development of additive manufacturing, research on lattice structures has focused mainly on process and design methods for structural development, and not on the repair of lattice structures. In the present study, the repairability of lattice structures was studied to extend the lifetimes of lattice-structured products; this would enable the reuse of products and induce people to directly get involved in creating a circular economy. To determine the factors to be considered for repairing lattice structures, standard specimens fabricated in the form of single undivided and adhesively bonded joint samples were fabricated by fused deposition modelling, and compared under four quasi-static tests: compression, tensile, shear, and three-point bending. The octet-truss unit cell was used in the specimen with a strut diameter of 1–2.5 mm at 0.5 mm intervals and a length of 10 mm. The difference in mechanical response between the two groups was significant in the tensile and three-point bending tests, while the compressive and shear tests showed similar results. Therefore, determination of the direction of the stress imposed on the products is essential for the proper repair of the underlying lattice structures, prolonging the life cycle of the product and thus leading to a positive effect on the circular economy.

Key words: lattice structure, octet-truss, additive manufacturing, mechanical response, repairing, circular economy.

1. Introduction

The concept of a circular economy involves forming a closed loop of resources, as opposed to a linear flow in the economy. A circular economy aims to maintain the maximum economic value of a product or material while minimising the environmental impact. This is achieved by extending the life of products and materials through a loop of repair, reuse, remanufacturing, and recycling (1–4). As illustrated in Fig. 1, inner circles (e.g., repair and reuse) are considered more economical because limited resources (e.g., energy, material, labour, etc.) are needed (5, 6). Therefore, in order to minimise the environmental impact, the key idea is to maintain the product in a condition similar to its original state, thereby enabling prolonged use (1, 2, 5). Although lattice structures, which determine lightweight characteristics and controllable mechanical properties, are being studied in many fields with the development of additive manufacturing (AM) technology (7–9), their characteristics (e.g., porous structure and mechanical response for specific applications) lead to difficulty in repair or reuse. Furthermore, although the materials used for fabricating the lattice structure in AM can be recycled, the use of additional energy and resources for recycling can lead to a loss of economic value (5, 6, 10–12). Therefore, this study was designed to explore the repairability of lattice structures in a circular economy.

Ensuring the strength and stiffness of materials while reducing the weight of products is one of the main advantages of tailoring the underlying lattice structures (13,
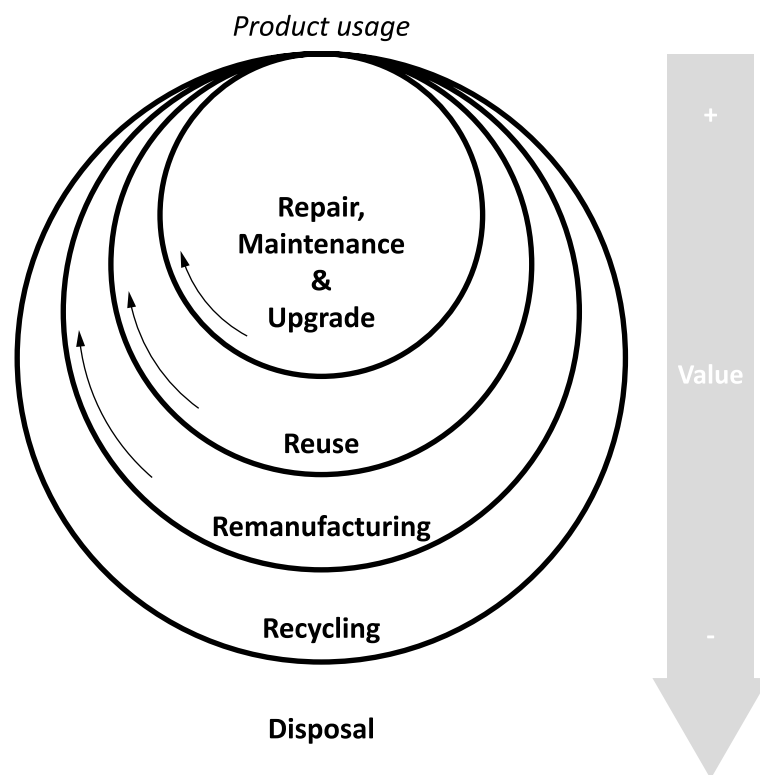
Fig. 1 Closed loop for product life cycle (5). The inner circle requires less resources and energy, resulting in more economical.

14). These features of lattice structures meet the needs of the society to conserve energy and reduce the use of materials (8). Hence, lattice structures have been researched and developed in various fields, including aviation, automobiles, thermal engineering, medical, etc. (15–18).

The development of AM technology has allowed the production of lattice structures with different materials that are tailored for various applications, contributing to the widespread use of AM in various domains (7–9). As a result, the design and production of lattice structures, including the development of the design methodology and lattice structure design for AM, has received considerable attention (9, 13, 14, 19–22). The use of AM not only provides freedom in design but also reduces the manufacturing time and wastage compared to conventional manufacturing processes (8, 9). However, despite significant interest in lattice structures, research regarding their repair is scarce.

For repairing lattice structures, problems and limitations caused by the complexity of the structures are easily detectable. (e.g., irregularity of damaged parts and lack of contactable surface area). In addition, as a repeating unit of complex structures, lattice structures are mainly manufactured in a single piece without joints, thereby eliminating the assembly process, which is an advantage of the AM method (23). These characteristics of the structure and manufacturing process result in problems in repair; however, there are methods to repair lattice structures.

Directed energy deposition (DED) is suitable for repairing metallic lattice structures because the technique can repair additively manufactured products with complex structures (23, 24). Modularisation of the lattice structure can also be employed in repairing the structure by replacing the damaged parts with new ones. Jenett et al. (25) developed modularised unit cells with a lattice structure that can be connected to certain joints, such that the damaged modules can be replaced by new ones if some parts are damaged. Xu et al. (26) developed a reconfigurable strut chain that can be assembled into a lattice structure, where only damaged struts need be replaced for repair, thus minimising the wastage of the material. Previously, repairable lattice structures have been fabricated using 2D struts (27–29), in which there are diverse types of assemblies depending on the size and shape of the unit, such as snap-fit, bonding, and brazing. However, the DED system demands specialised knowledge and skills as it is a relatively new technology (24), whereas all modularised lattice units require assembling in production, thus weakening the aforementioned advantages of AM. In addition, there is a limit to the form that is possible with the fixed shape of modularised units; the size of the unit cells also need to be sufficiently large to be assembled, thereby making the process comparatively more suitable for large objects. Moreover, all modularised units are not easily disassembled and reassembled; the ease of disassembling and reassembling depends on the

method of joining of the structures. For foam structures, which are also a type of cellular structure (14), there are several techniques of joining porous parts: soldering, brazing, gluing, welding, screwing, and bolting (30). However, owing to the characteristics of foam structures, which consist of holes of irregular size and shape, there are limitations on joining different parts. Solder can flow into the structure during soldering; similarly, adhesive can flow into the structure during gluing. In addition, joints can become stronger or weaker than the foam structure depending on the type of joining or the quantity of adhesives that are applied in certain regions (30–32). Brazing and welding require special tools and techniques, and are usually used for joining with flat sheets in order to fabricate foam core panels (30, 33). Various alternative joining methods that are used for solid products can also be used to join lattice structures as they are cellular structures with a certain regularity. These methods include bonding, cold-welding, hot-welding, threading, and snap-fit.

As lattice structures can possess a variety of mechanical properties depending on their structure and usage (9), incorrect repair can shorten the life of products. There-
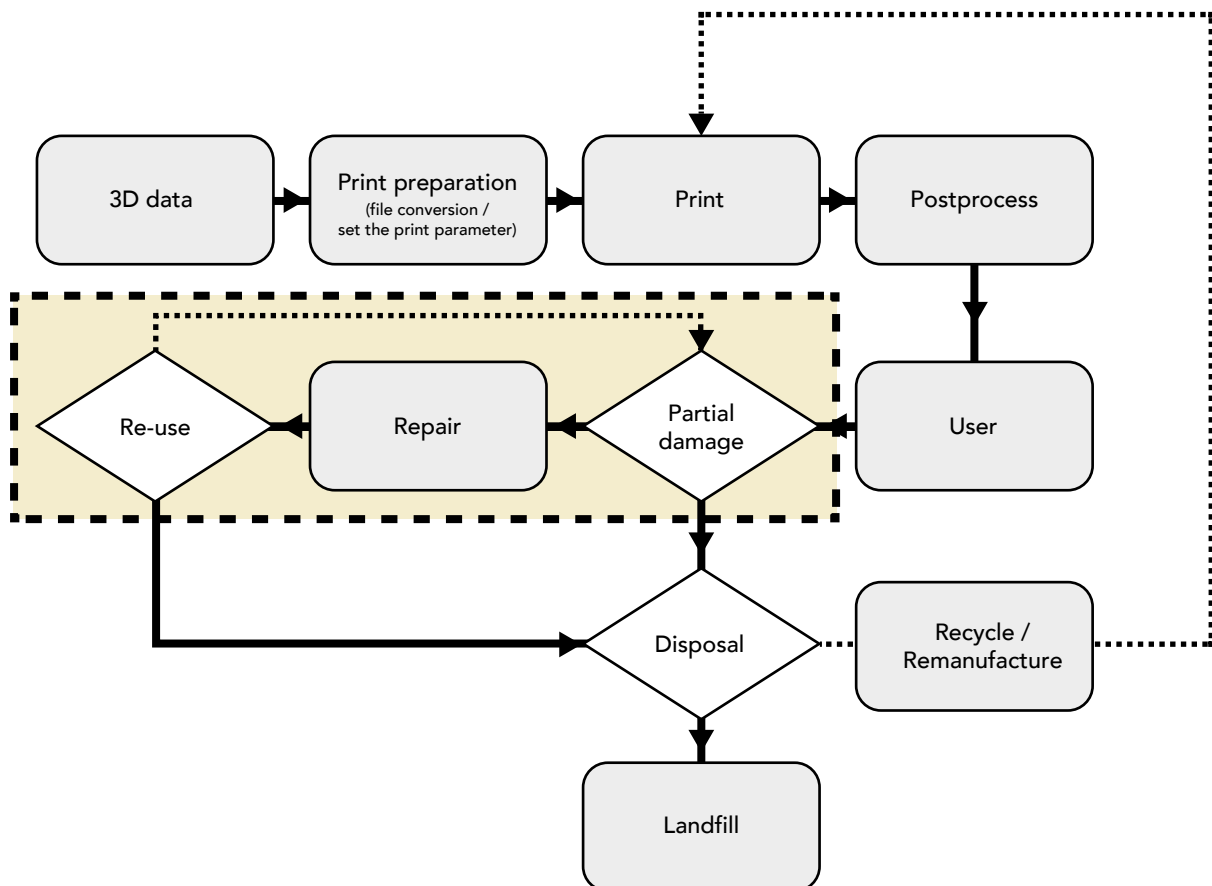
Fig. 2 The life cycle of the additively manufactured lattice structure. The flow shows how the lattice structure is produced and consumed. The highlighted section is added on the current workflow of lattice structured product life cycle in order to extend the product lifespan by proper repair of the damaged parts, enhancing the circular economy. The figure adapted from the circular economy model by Ellen MacArthur Foundation (3).

fore, it is crucial to reproduce the same parts with the previous undamaged state in order to achieve the same mechanical response. Consequently, accurate methods and guidelines for repairing lattice structures are required to aid the development of circular economies.

Thus, the aim of this study is to investigate the factors to be considered when repairing the lattice structures in order to contribute to circular economies by enhancing the entities as highlighted in Fig. 2. Hence, consumers can be involved in repairing products and creating inner circles in the closed loop, which can play an important role in product life extension (34).

To maintain the original usability of the lattice structure, the repaired parts should have the same or similar mechanical properties as the original. To repair the lattice structure, the damaged parts should be identified accurately to reproduce identical shaped parts. Additionally, they must be printable with a 3D printer, easily reassembled and remanufactured with accessible and editable data. The complete list of requirements (LoR) is listed in Appendix A.
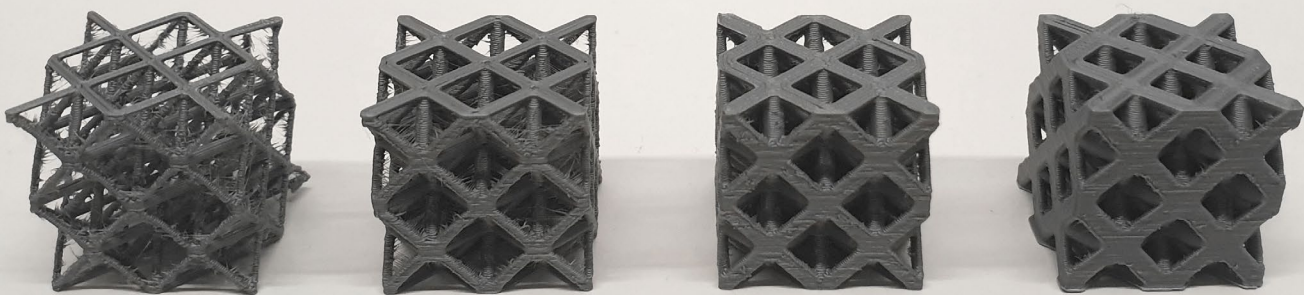
Octet-truss lattice structure with the different strut diameters.

2. Method

Strut-and-node-based lattice structures have considerable potential as they allow users to design the shape, size, and number of struts to suit their objective (19, 35). This is in contrast to the triply periodic minimal surfaces (TPMS), for which users can only adjust the size and thickness of unit cells because of their fixed shape (19). Strut-and-node-based unit cells can be divided into stretch-dominated and bending-dominated unit cells (36). Stretch-dominated structures are the most widely used wherein lightweight traits as well as a certain stiffness are required (35). Thus, for the tests, the octet-truss was selected as the unit cell geometry of the lattice structure; the octet-truss has been widely examined in stretch-dominated lattice structures (37–39).

Each strut of the lattice was fixed at 10 mm, which was the length of the unit cell within the range of mesoscale lattice structures from 0.1 mm to 10 mm (13, 19). Four different sizes were used for the diameter of the strut: d = 1.0, 1.5, 2.0, and 2.5 mm.

2.1. Specimen design

There are various methods to test the adhesion strength. To measure the stress in adhesive joints, compressive, tensile, shear, peel, and cleavage are generally utilised (40), and a large number of standards have been created. However, there is no specific standard for measuring the adhesion strength corresponding to the mechanical properties of the lattice structure. Therefore, in this study, the specimens for the tests were modified based on the American Society for Testing and Materials (ASTM) and International Organization for Standardization (ISO)(41), and the specimen designs of relevant studies (42, 43) were referred to.

Four different types of specimens were designed for each test: compressive, tensile, shear, and three-point bending. To compare the mechanical behaviour of the repaired lattice structure with the original state, one specimen was fabricated as a single piece (standard specimen), while the other was joined with two separate parts (joined specimen). The separate lattice parts were glued together by a Loctite

Table 1

Specification of the adhesive used in tests.

Performance Properties	Configuration
Fixture Time (sec)	30
Cure Time (h)	12-24
Cured Form	Brittle solid
Tensile Shear Strength (MPa)	2-20

plastic adhesive with an activator, which was selected based on the adhesion test, as discussed in Appendix A. The specifications of the adhesive are listed in Table 1. Six specimens were used for each parameter set because low consistency is one of the characteristics of fused deposition modelling (FDM) technology (23, 43).

To measure the compressive response of the bonded lattice structure, the ASTM D1621 (41) standard was modified, which is the standard for the compressive prop-

front   side   front   side
(a)   (b)
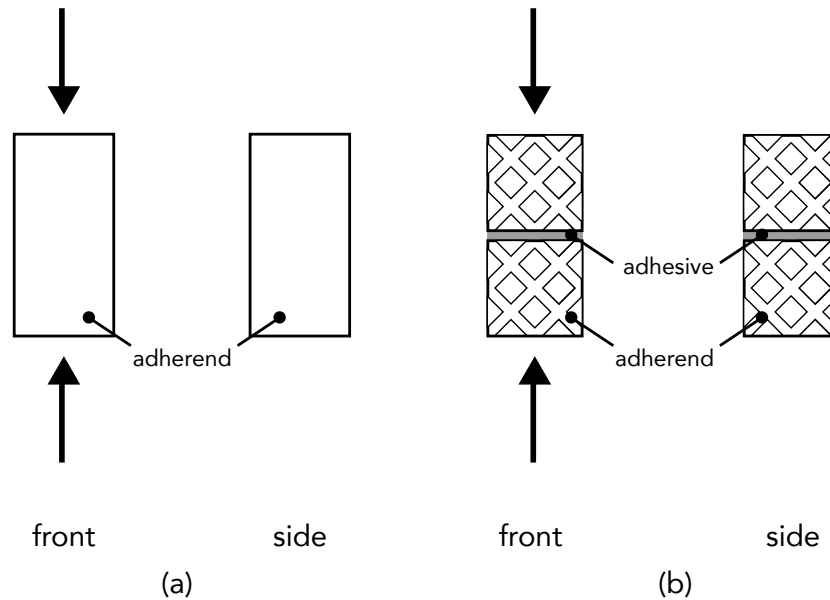
Fig. 3 Schematic representation of the compression specimen; (a) standard and (b) modified.

front   side   front   side
(a)   (b)
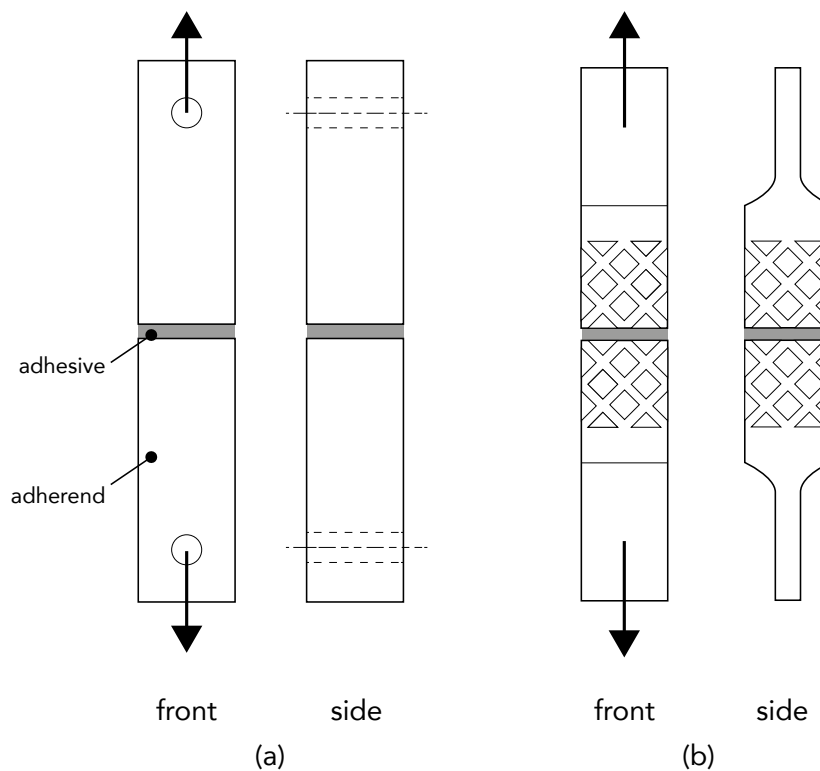
Fig. 4 Schematic representation of the tensile (butt-joint) specimen; (a) standard and (b) modified.

erties of rigid cellular plastics (see Fig. 3).

For the tensile test, the specimen was modified based on the specimen design from a previous study (42, 43), and the ASTM D2095 (44) standard was referenced for testing the adhesion between the two parts, as depicted in Fig. 4.

As illustrated in Fig. 5, the specimens for the shear test were modified based on the ASTM D5656 (45) and ISO 11003-2 (46) standards, which are the standards for thick adherends. Similar to the tensile test, the specimen was bonded to the same
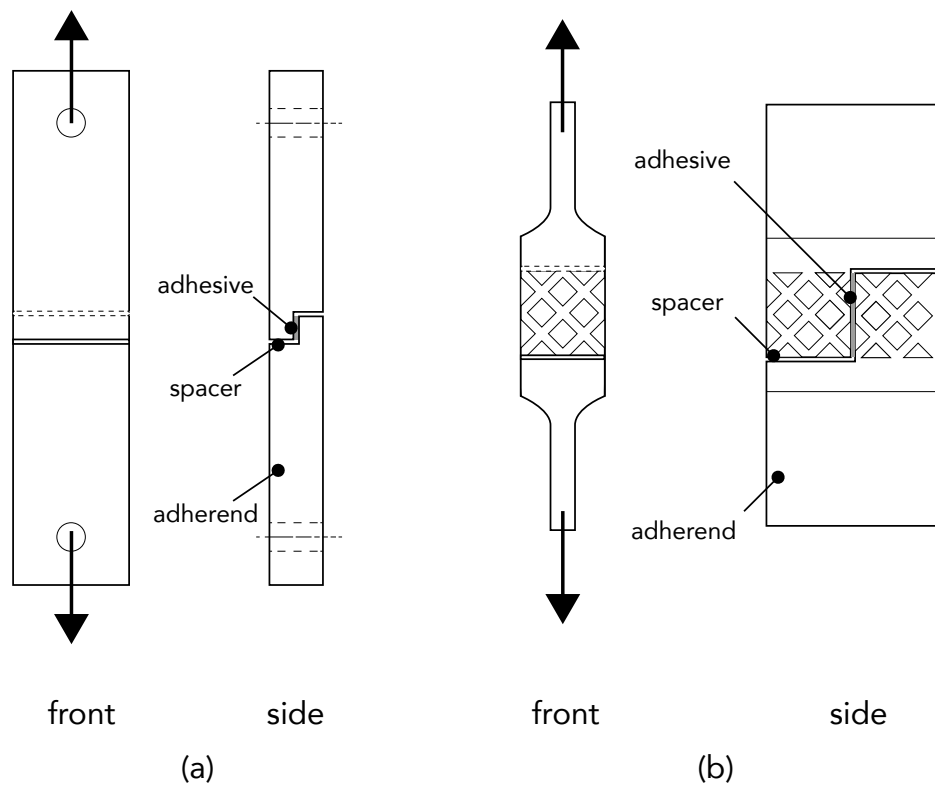
Fig. 5 Schematic representation of the shear specimen; (a) standard and (b) modified.
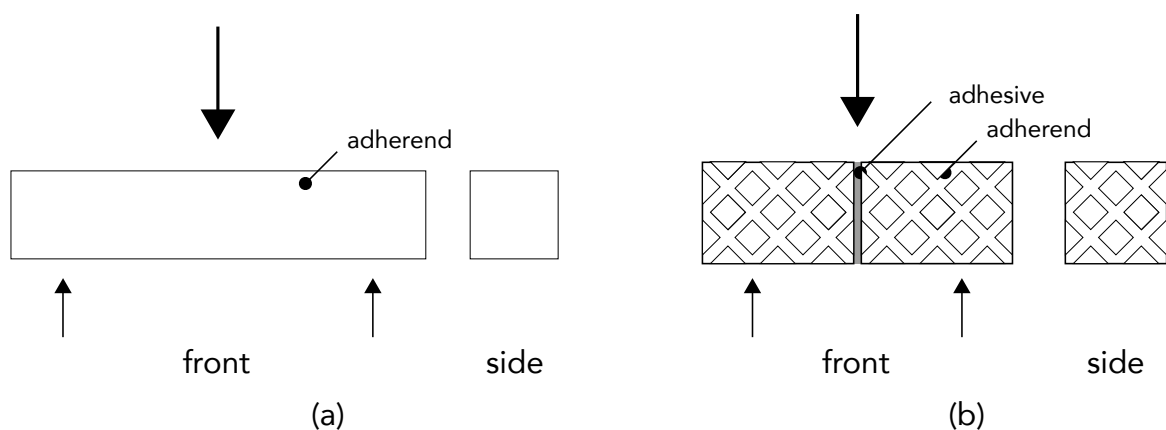
Fig. 6 Schematic representation of the three-point bending specimen; (a) standard and (b) modified.

surface area, and the original specimen was printed in a single piece.

In the specimen design for the three-point bending test, a previous three-point bending test with an octet-truss (47) was referred along with the ASTM D790 standard (48). Fig. 6 shows the designed specimen based on the study and the standard, which is applicable for the rectangular bar specimen.

2.2. Fabrication

All specimens were designed using Fusion 360 software and transferred to STL format by Slic3r. An FDM 3D printer (Prusa i3 mk3) with polylactic acid (PLA) filament was used to fabricate the designed specimens. The same printing parameters were used to fabricate all the specimens to ensure identical mechanical properties for the structures (23). The detailed printing parameters for the fabrication of the specimens are shown in Table 2. All specimens for each test were printed in the same direction as the printing direction significantly affects the mechanical behaviour (49). The detailed specifications of all the specimens are listed in Appendix B.

In the case of the joined specimens for the tensile and three-point bending tests, the bonding surface was uneven because of the layer created by the printing direction. Therefore, a grit size of 280 sandpaper was used to abrade the surface (50), resulting in a surface roughness of 3–6 μm (51), Additionally, all contaminants such as dust and debris on the surface of the joint were removed in order to improve the tensile strength (52). After trimming, the adhesive was applied and cured for 24 – 36 h.

Table 2

Configuration of printing parameters.

Printing parameters	Configuration
Printing temperature (℃)	215
Print speed (mm/s)	100
Infill (%)	100
Layer height (mm)	0.15
Filament diameter (mm)	1.78
Nozzle diameter (mm)	0.4

2.3. Experiments

Four quasi-static tests were carried out to compare the mechanical behaviour of standard specimens with joined specimens. The compression, tension, shear, and three-point bending tests were conducted sequentially. Zwick Roell Z010 was used in all tests with a 10 kN load cell, and the loading speed for each test was set according

to each ASTM standard listed in Section 2.1.

The quasi-static compression test for a total of 48 standard and joined specimens was conducted at a loading speed of 2 mm/min, following the test standard of ASTM polymer compression. For the quasi-static tensile and shear tests, a loading rate of 1 mm/min was set; a loading rate of 0.5 mm/min was used for the three-point bending test with a loading nose diameter of 10 mm. The loading nose was arranged at the centre of the specimens with a supporting span of 40 mm, allowing each end to have a 10 mm overhang. All the specimens were located precisely at the centre of the machine; the test stopped when either the reaction force reached 10 kN or the force was less than 80% of the maximum force. The deformation process of the specimens was recorded, and the force–displacement curve was extracted from each test.

2.4. Application of the results

The results obtained from the tests were applied to consumer products with lattice structures, thus demonstrating the method of application of results to repair lattice structures. Products were selected that could reflect the design of the experiment well, rather than those that are sold or used commercially. The same size and geometry used in the experiment were utilised to demonstrate the application. Finally, the repairing examples were adapted to a circular economy model to evaluate the impact of repair of 3D printed lattice structures on the circular economy.
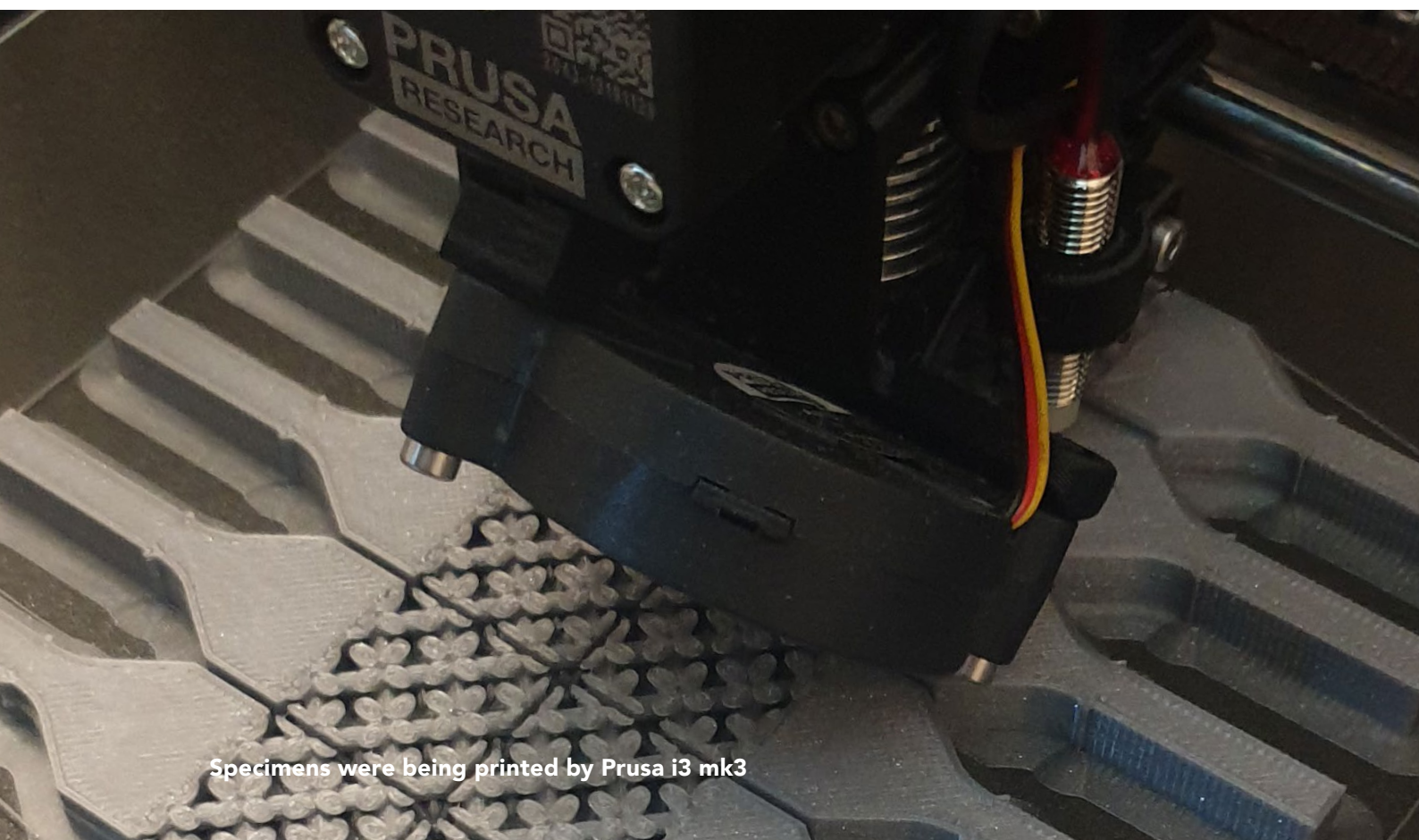
Specimens were being printed by Prusa i3 mk3

3. Results

The reaction force P and the displacement ΔL obtained from the test were divided by the effective area A and the original height of the specimen L, respectively, to obtain the engineering stress (σ)–engineering strain (ε) curve.

$$\sigma = \frac{P}{A} \tag{1}$$

$$\varepsilon = \frac{\Delta L}{L} \tag{2}$$

In accordance with Hooke's law, the Young's modulus was determined by the slope of the elastic region in the stress–strain curve, and the yield strain was measured at 0.2% plastic strain for both standard and joined specimens. However, when buckling fracture of the lattice strut or adhesive bond failure occurred within the linear elastic region, the point of failure was considered to be the yield stress. The Young's modulus and yield strength values of six specimens for each test parameter were averaged and these values are listed in Appendix C.

3.1. Mechanical response of compression tests

As shown in Fig. 7(e) and (g), the deformation always initiated at the middle layer of the standard specimens if the strut diameters were 2.0 mm and 2.5 mm. Five out of the six joined specimens were not deformed from the middle of the specimen because of the glued joints (see Fig. 7(f) and (h)). This influenced the mechanical response.

In addition, for the standard specimens, each layer showed a relatively consistent deformation process, while those of the joined specimens showed an inconsistent mechanical response and a plateau stage throughout the graph. As a result, as observed in Fig. 8(a)–(b), the standard specimens were uniformly deformed as compared to the joined specimens after the test.

When the strut diameter was 1.5 mm or less, the mechanical behaviour between the standard and joined specimens was not noticeably different (see Fig. 7(a)–(d)). For a strut diameter of 1.5 mm, both groups were not significantly affected by the joint due to the buckling fracture of the struts. With a specimen strut diameter of 1.0 mm, both groups of specimens were broken and bounced off irregularly during the test (see Fig. 7(a) and (b)).

Regardless of the diameter of the strut, the joined specimens had a slightly lower compressive modulus and yield strength than the standard specimens, but most of the results were within the standard deviation (Fig. 9). There were minor variations in the detailed deformation process when the strut diameter was 2.0 mm or more.
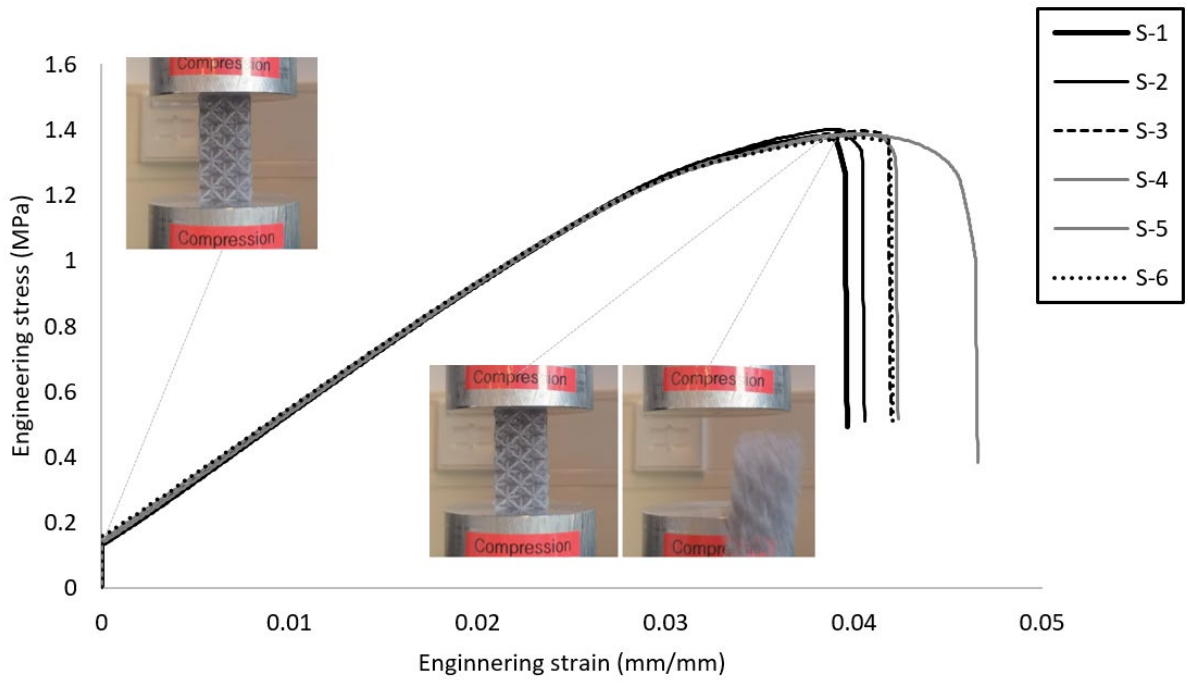
(a)
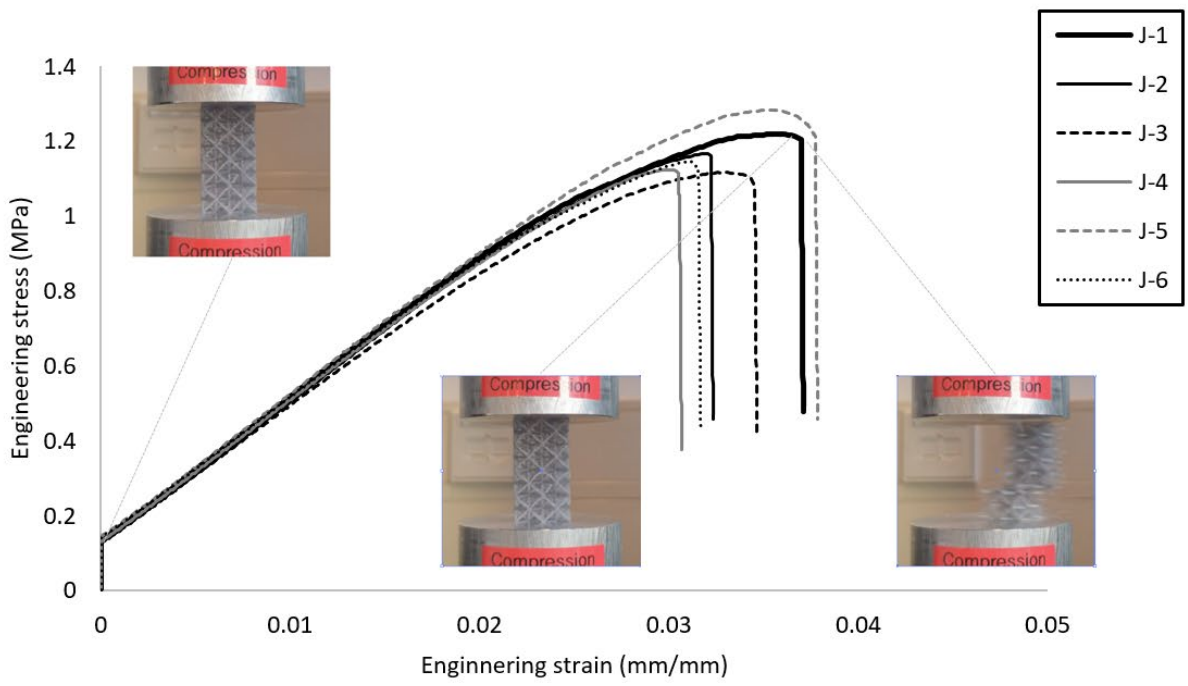
(b)
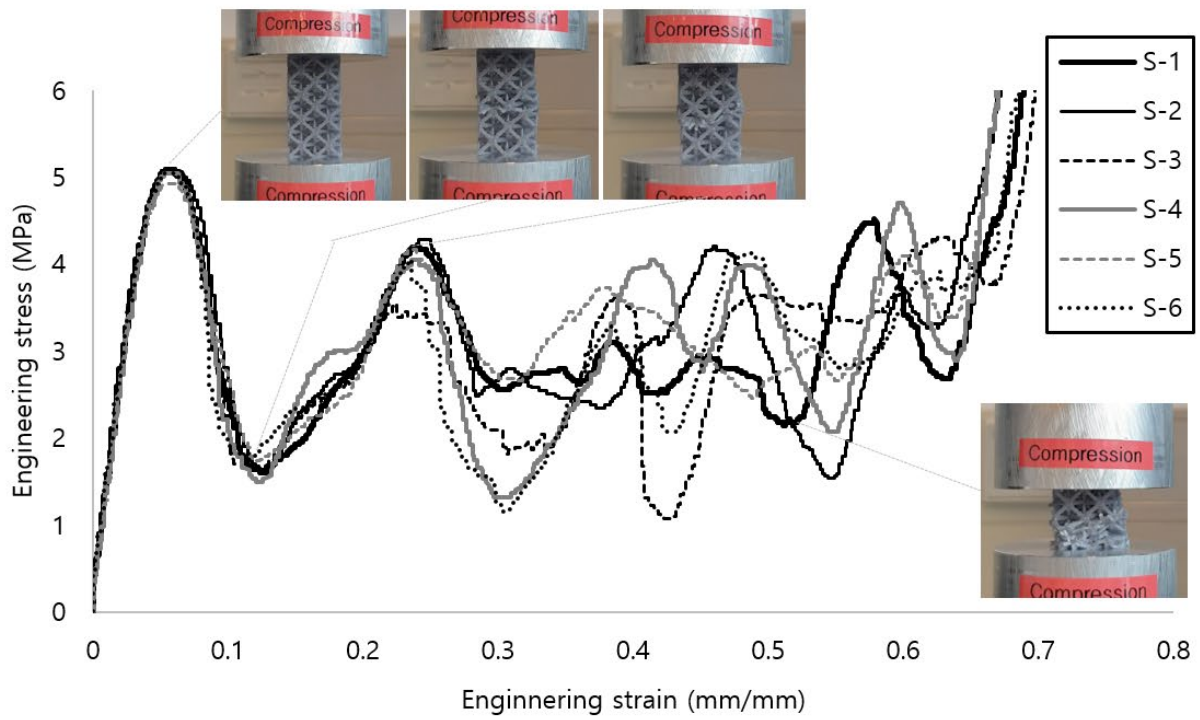
(c)
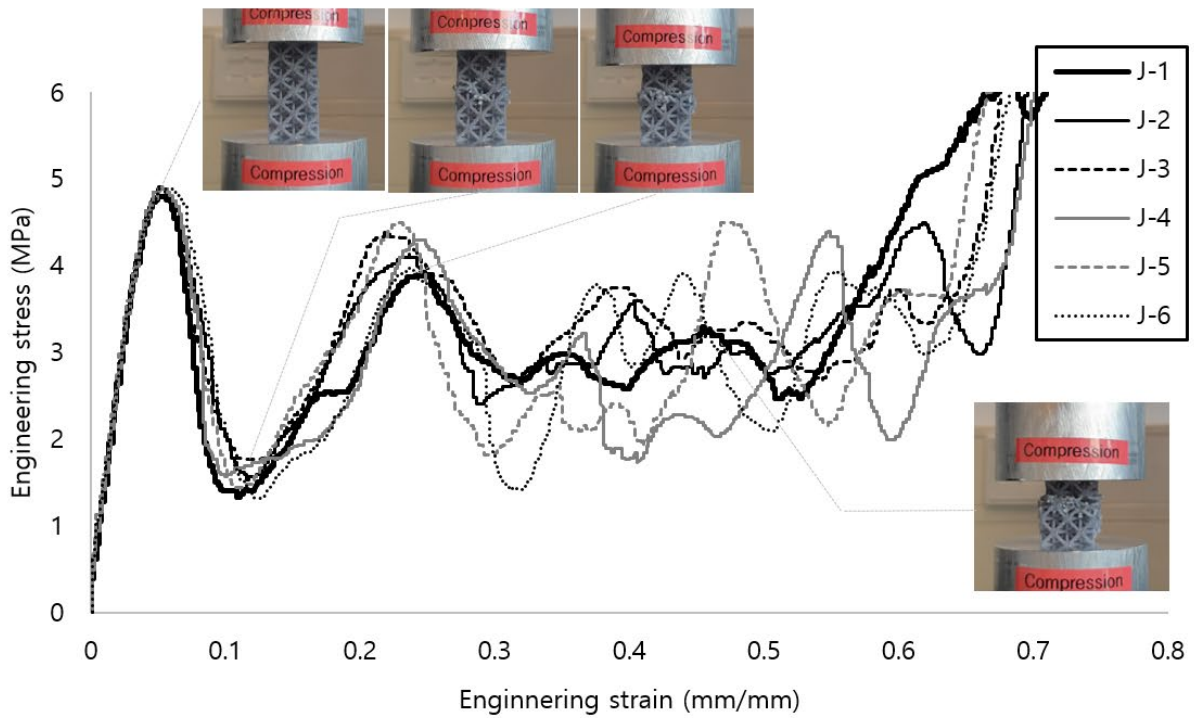
(d)
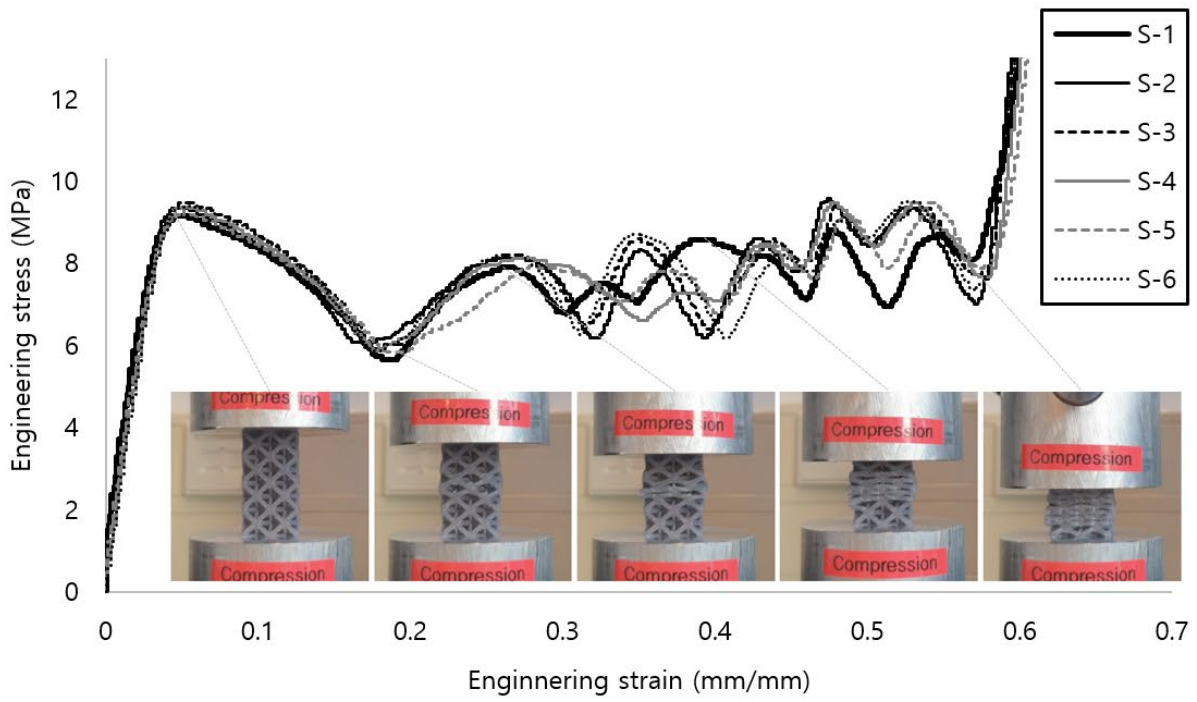
(e)
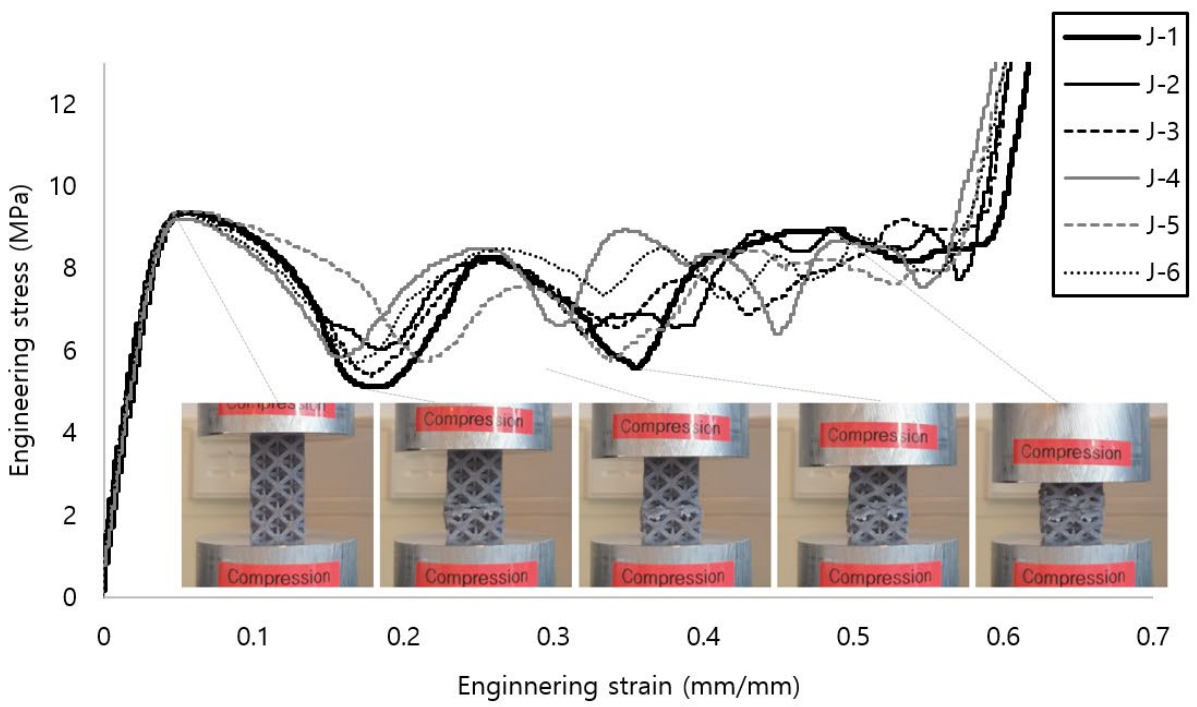
(f)
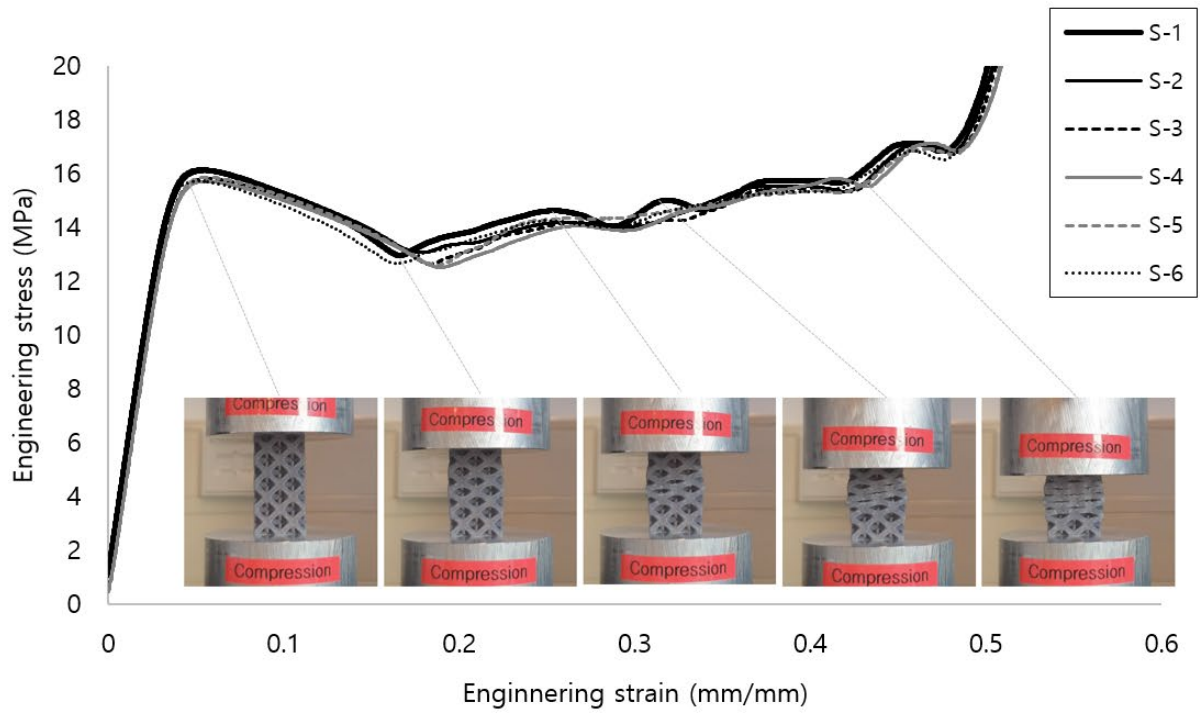
(g)
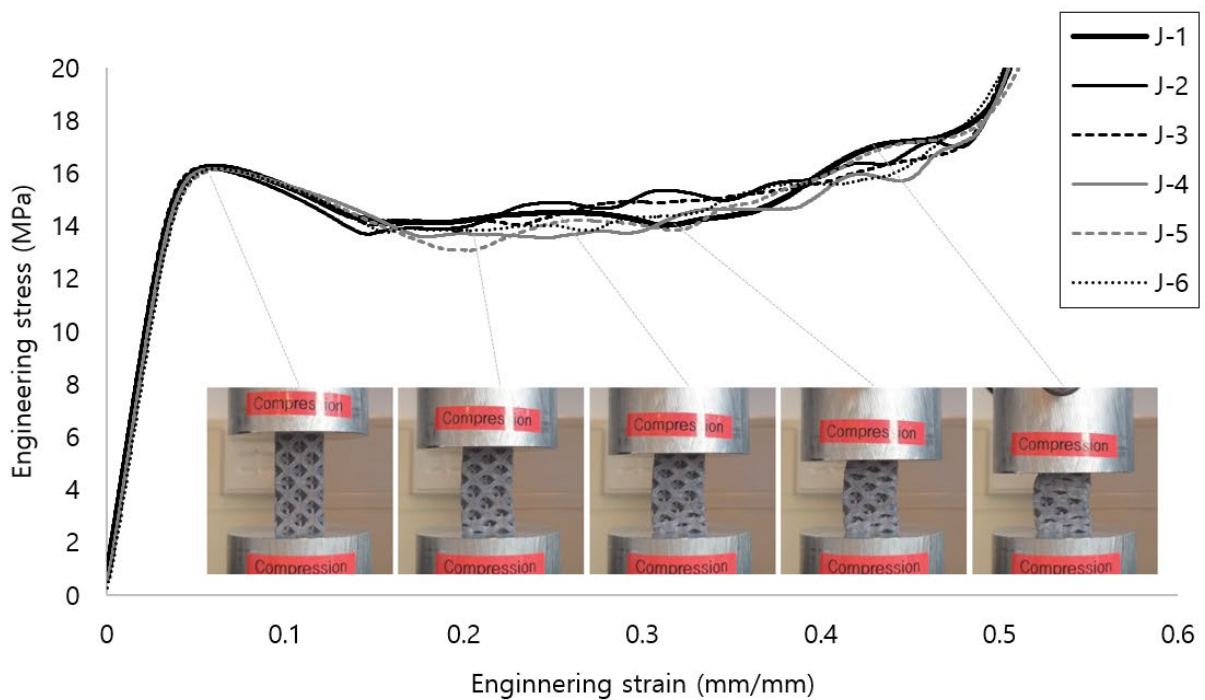
(h)

Fig. 7 Compressive stress-strain curve with the corresponding images of deformation process: (a) standard specimen, d=1.0mm; (b) joined specimen, d=1.0mm; (c) standard specimen, d=1.5mm; (d) joined specimen, d=1.5mm; (e) standard specimen, d=2.0mm; (f) joined specimen, d=2.0mm; (g) standard specimen, d=2.5mm; (h) joined specimen, d=2.5mm.
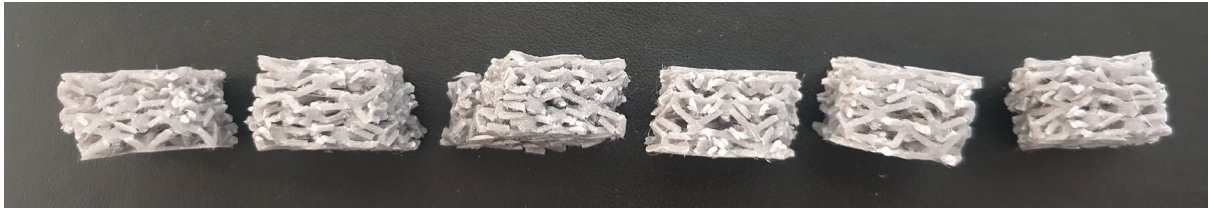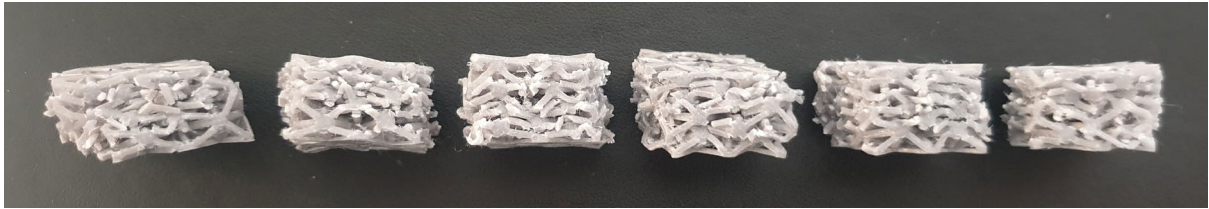
Fig. 8 Deformed specimens after the compression test: (a) standard specimen, d=1.5mm; (b) joined specimen, d=1.5mm; (c) standard specimen, d=2.0mm; (d) joined specimen, d=2.0mm; (e) standard specimen, d=2.5mm; (f) joined specimen, d=2.5mm.
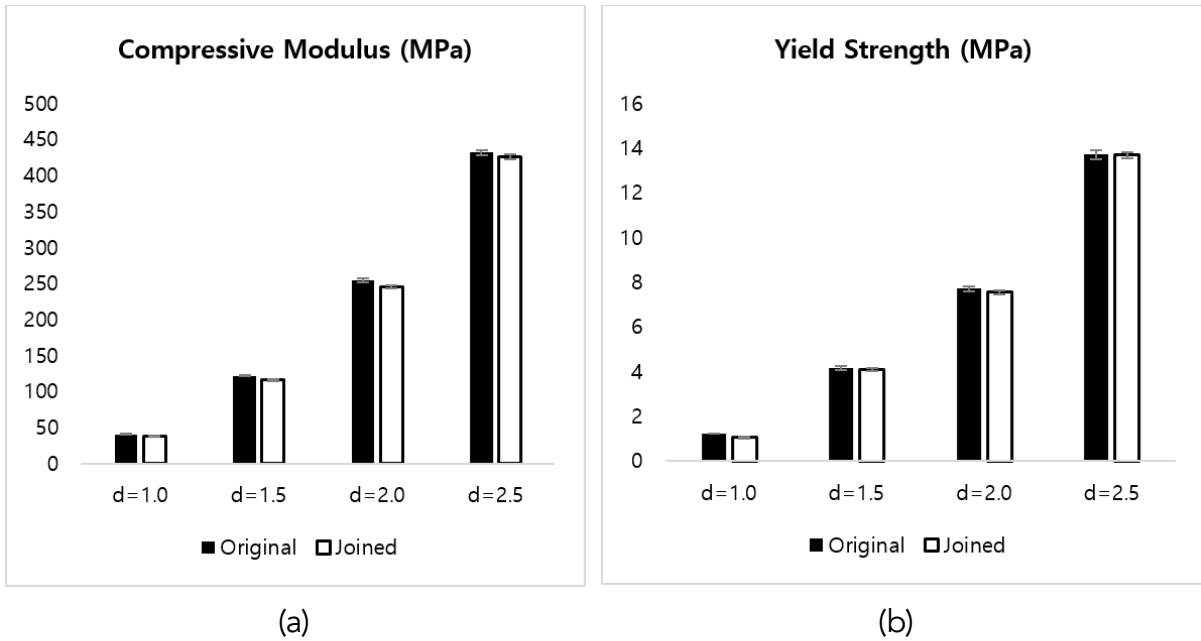
Fig. 9 Compressive modulus and yield strength of both standard and joined specimens with four different strut diameters; (a) compressive modulus and (b) yield strength.

3.2. Mechanical response of tensile test

Unlike the compression test, the tensile test showed an observable difference between the standard and joined specimens. As observed in Fig. 10, the standard specimen was split into two as the struts were broken during the tensile test, while the joined specimen showed cohesive failure. However, for the joined specimen, when the strut diameter was 1.5 mm, few struts broke before cohesive failure, and
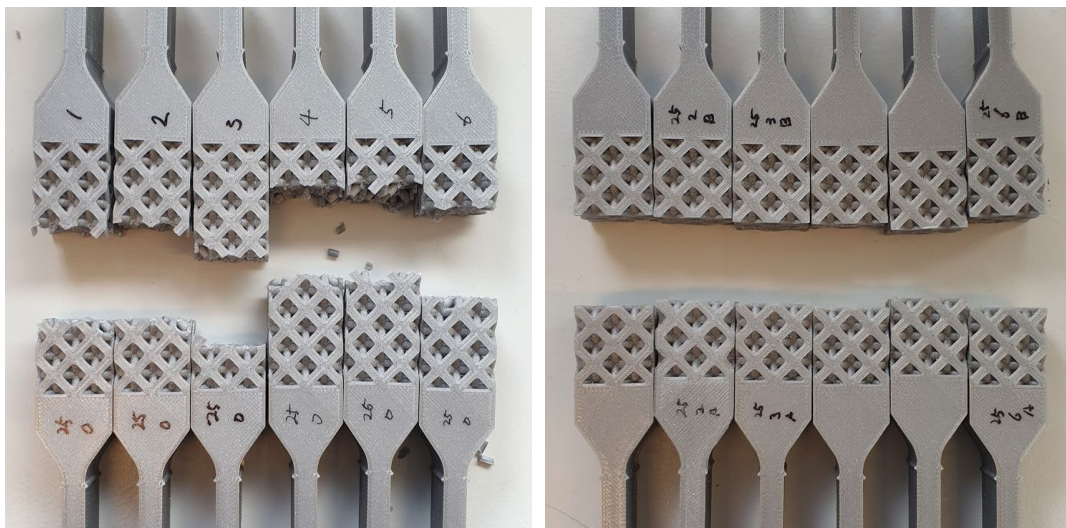
Fig. 10 Images of tensile specimens after fracture: (a) standard specimen, d=2.5mm; (b) joined specimen, 2.5mm.
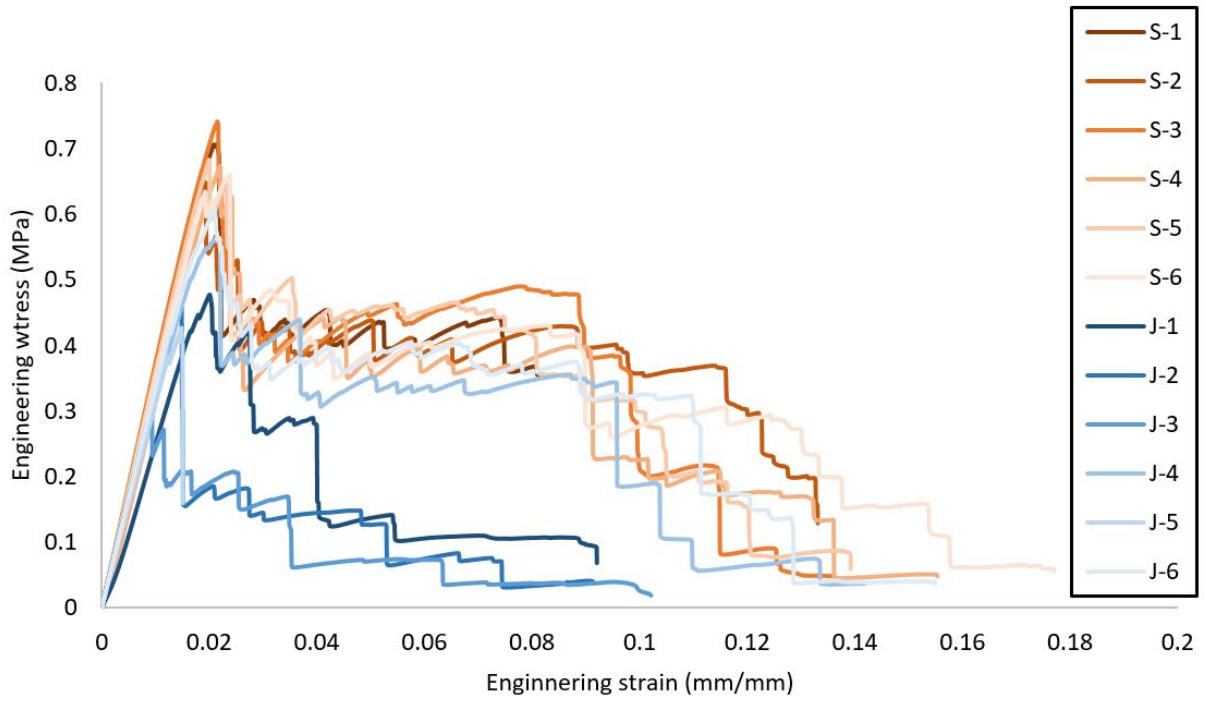
(a)
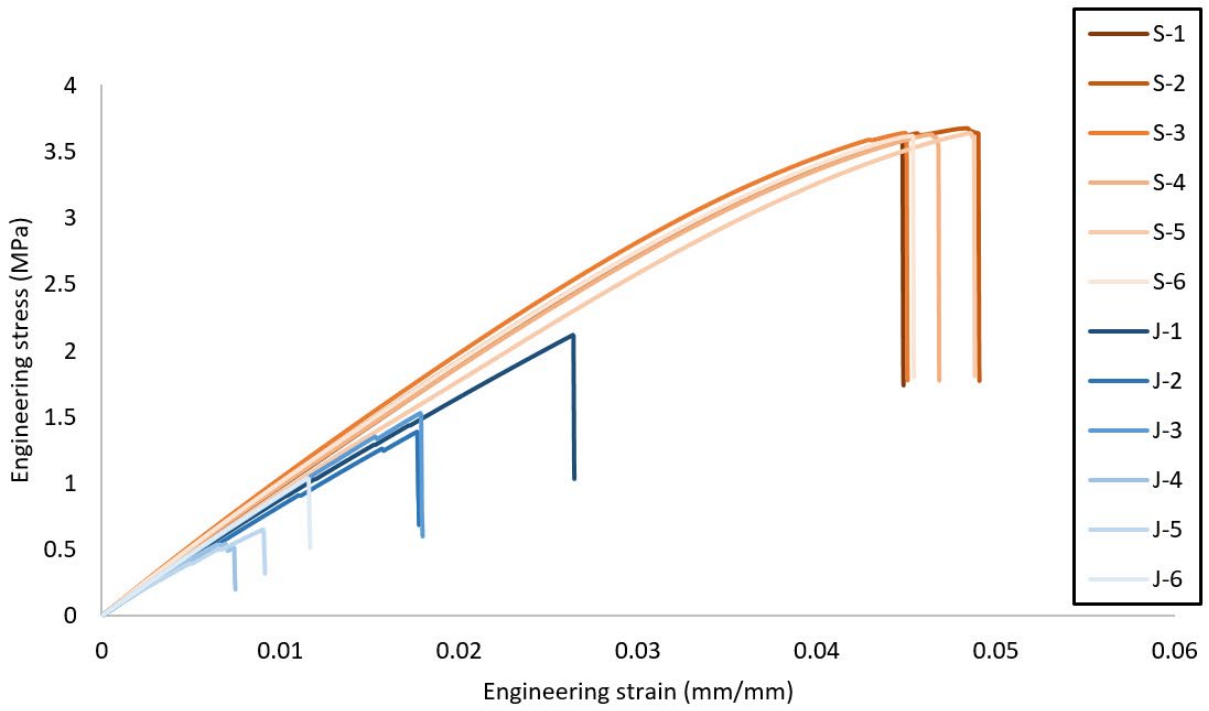
(b)
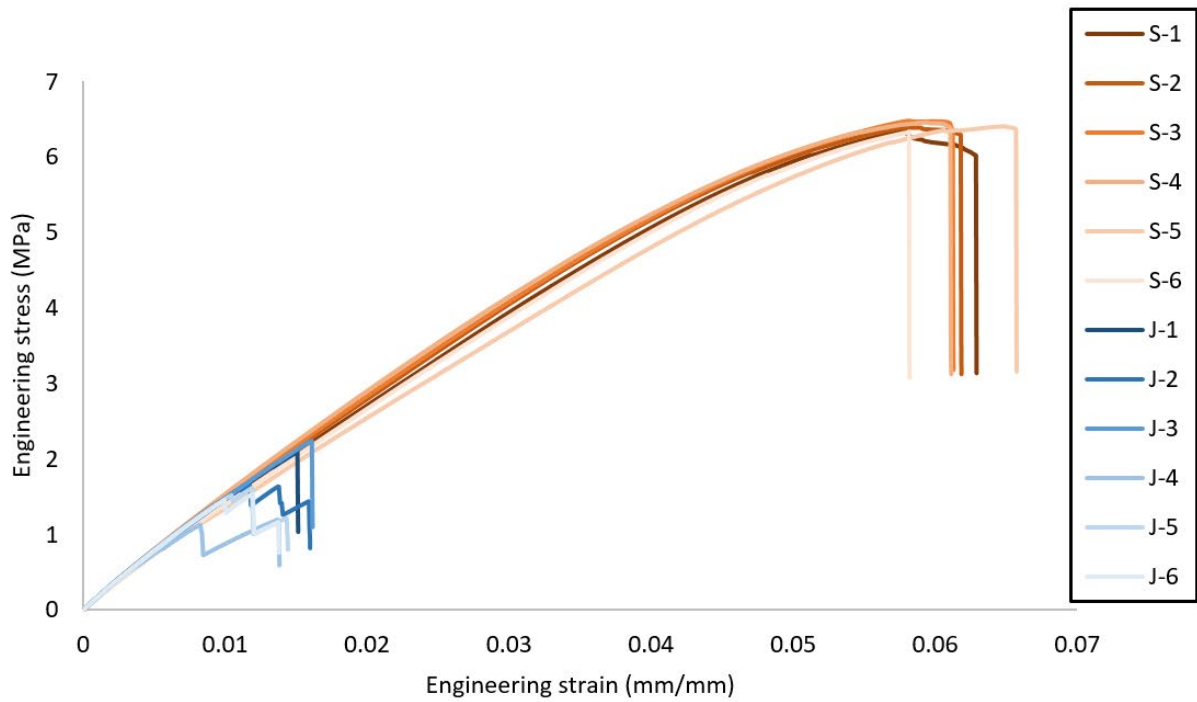
(c)
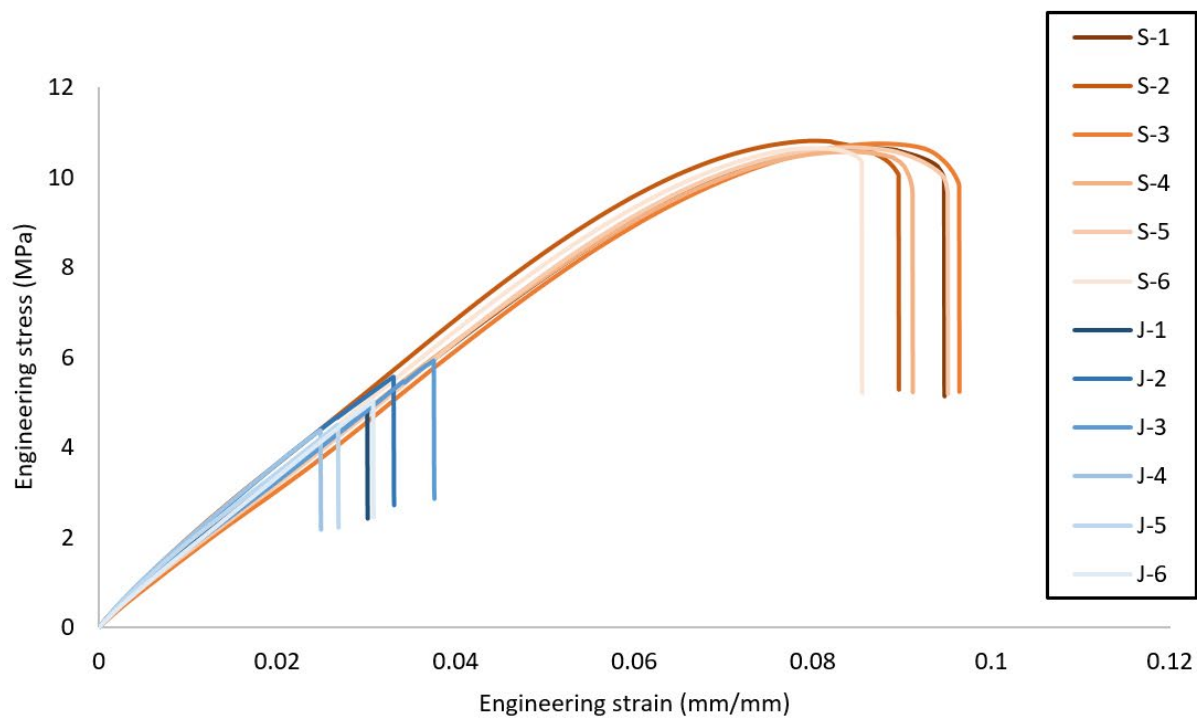
(d)

Fig. 11 Tensile stress-strain curve with the corresponding images of deformation process ('S' represents standard, 'J' represents joined): (a) standard and joined specimen, d=1.0mm; (b) standard and joined specimen, d=1.5mm; (c) standard and joined specimen, d=2.0mm; (d) standard and joined specimen, d=2.5mm.

23
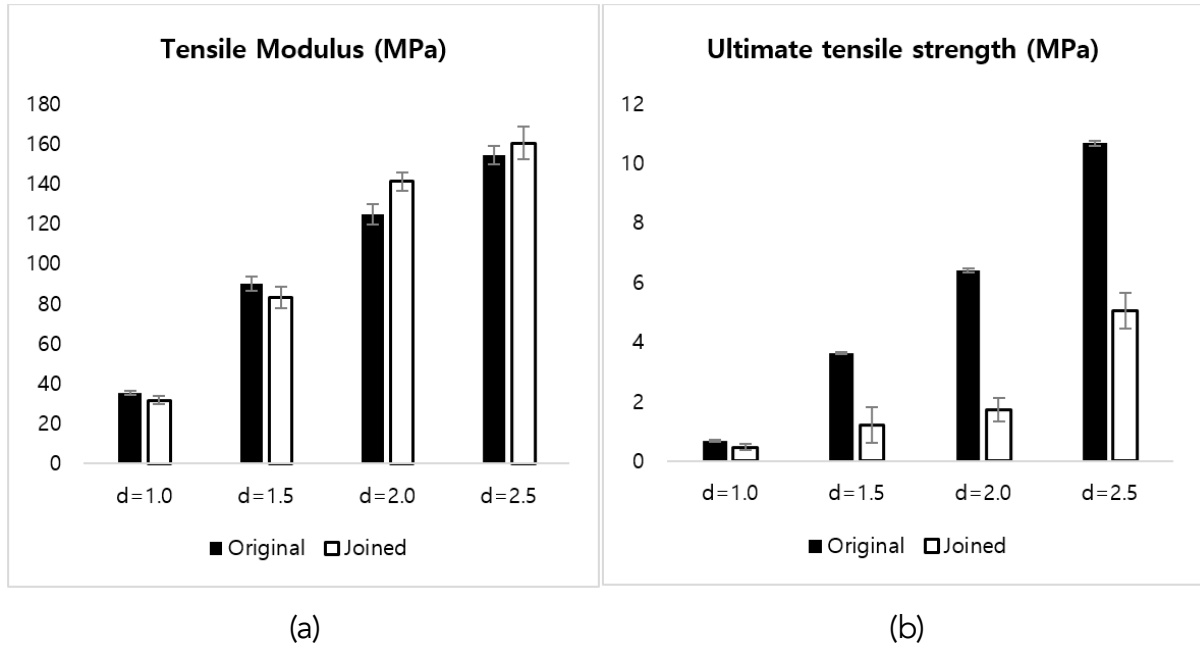
Fig. 12 Tensile modulus and yield strength of both standard and joined specimens with four different strut diameters; (a) tensile modulus and (b) yield strength.

two of the joined specimens with a diameter of 1.0 mm showed almost the same mechanical response as the standard specimens. Nonetheless, owing to the limited joint area due to the presence of the thin strut, the adhesive was not applied consistently, resulting in a large deviation between the results of the joined specimens.

As shown in Fig. 11 (a)–(d), both standard and joined specimens maintained a similar modulus of elasticity before the joined specimens underwent cohesive failure. However, as observed in Fig. 12, the tensile modulus of the joined specimens was slightly higher than that of the standard specimens when the strut diameter was 2.0 mm or more. This is because there was a discrepancy between the two groups regarding the length of the linear stage in the curves. The standard specimens had a longer linear region until the yield point (see Fig. 11 (c) and (d)), which resulted in their tensile modulus being slightly lower as the slope at the beginning of elastic deformation was slightly higher. Although the tensile modulus varied similarly, the yield strength showed a noticeable dissimilarity between the two groups (see Fig. 12).

Fig. 13 shows the relationship between the tensile modulus and tensile strength over the relative bonding surface area of each specimen. The relative joint areas were obtained by dividing the bonding surface area of the lattice specimens by those of the solid specimens:

$$A_{relative} = A_{sample} / A_{solid} \qquad (3)$$

The four solid specimens for each group were also fabricated and tested using the same parameters as the other specimens. The reaction forces for the standard spec-
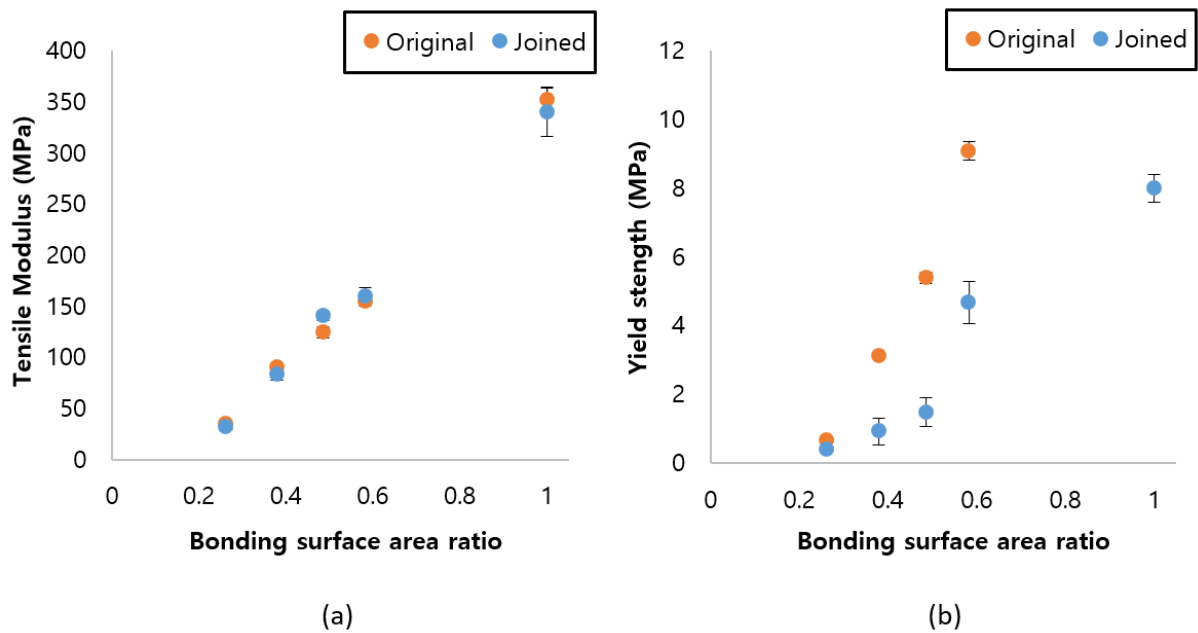
Fig. 13 The relationship between (a) the tensile modulus and (b) yield strength to the relative bonding surface area ratio for both groups.

imens were not measured as they exceeded 10 kN. The tensile modulus showed a linear trend with respect to the bonding surface area. However, although the tensile modulus increased with increase in the bonding surface area, the yield strength of the joined specimens did not increase at a constant rate (see Fig. 13 (b)). This is because the rate of increase of the volume and bonding surface area ratios gradually decreased as the strut diameter increased (see Fig. 15), resulting from the overlap of struts in a limited space, as observed in Fig. 14. In addition, as the strut diameter became thinner, the structure became ductile. Ductility caused the necking of the specimens, causing each strut to break irregularly before the breakage of the entire structure, as illustrated in the plastic region in Fig. 11 (a) and (b). Therefore, in order to clearly identify the relationship between the bonding surface area of the lattice structure and adhesion, it is necessary to increase the number of variables of the strut diameter in the test as the ductility affects the mechanical response (53).
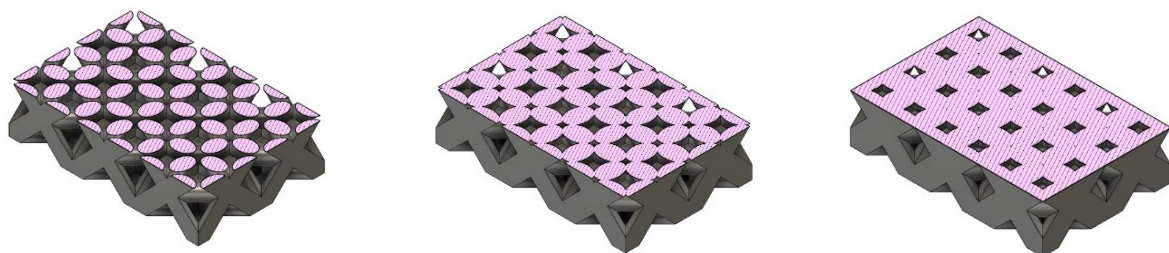
Fig. 14 The octet-truss lattice structure consisted of 10mm unit cell with the strut diameter of 2.5mm to 3.5mm. The struts start overlapping from the diameter of 3.0mm: (a) d=2.5mm; (b) d=3.0mm; (c) d=3.5mm.
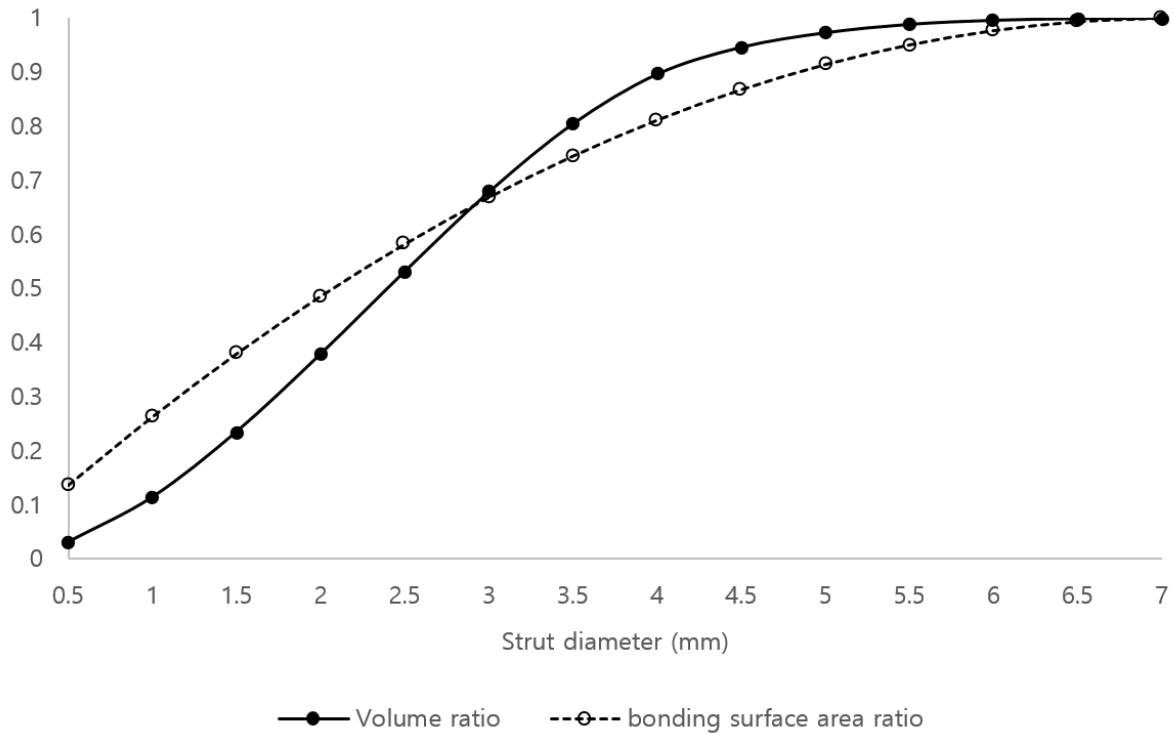
Fig. 15 The ratio of the volume and the bonding surface area from the strut diameter of 0.5 mm to solid at intervals of 0.5 mm.

3.3. Mechanical response of shear test

In the joined specimens, a slight deviation was observed between the curves compared to the standard specimens (see Fig 16), but the mechanical response was generally the same or within the standard deviation (Fig. 17). As observed in Fig. 16 (c) and (h), several specimens in the shear test showed partial structural or cohesive failure in the elastic region. However, as these failures did not seriously affect the overall mechanical response, they were ignored while determining the yield strength or shear modulus.

For the curves falling vertically, as shown in Fig. 16, the failure was not cohesive, but structural. The lattice struts of the joined specimens broke away similar to those of the standard specimens, regardless of whether they were glued (see Fig. 18). Similar to the tensile test, when the strut diameter was 1.0 mm, the struts of the specimen were partially broken and some of them were still attached as a result of the ductility imparted by the thin struts. With these features, the struts were inter-twined in the specimens (Fig. 19), thereby leading to the mechanical response in the plastic region as shown in Fig. 16 (a)–(b).
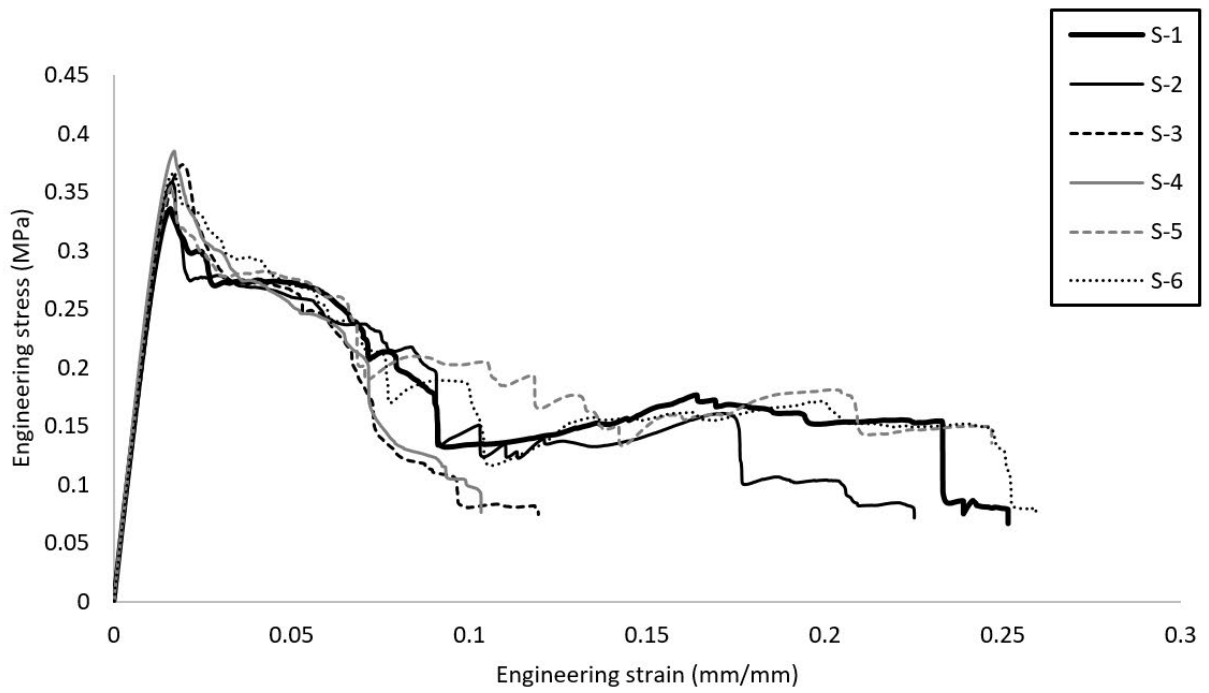
(a)
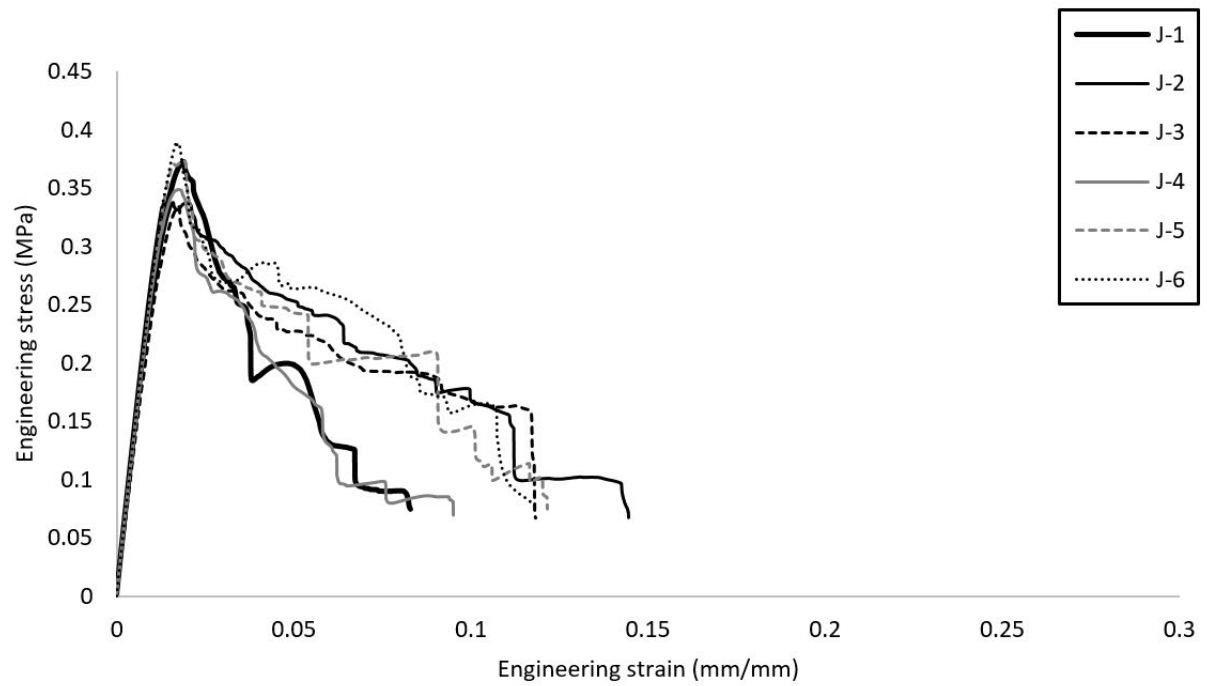
(b)
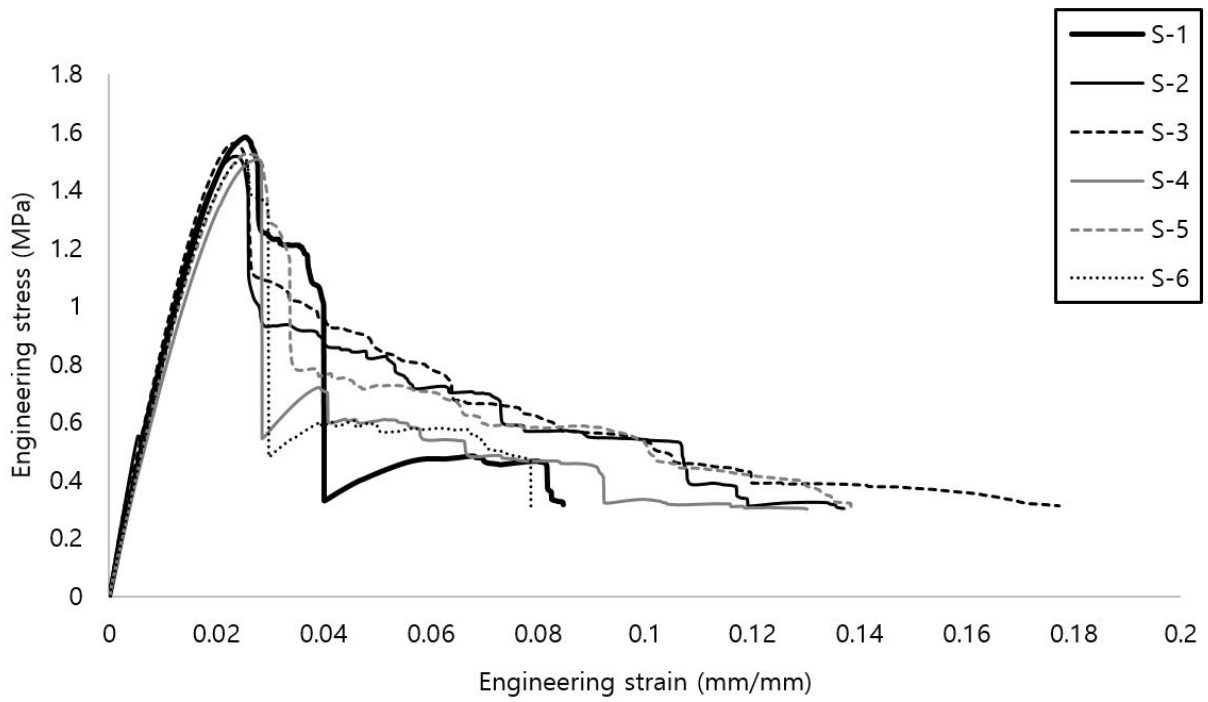
(c)
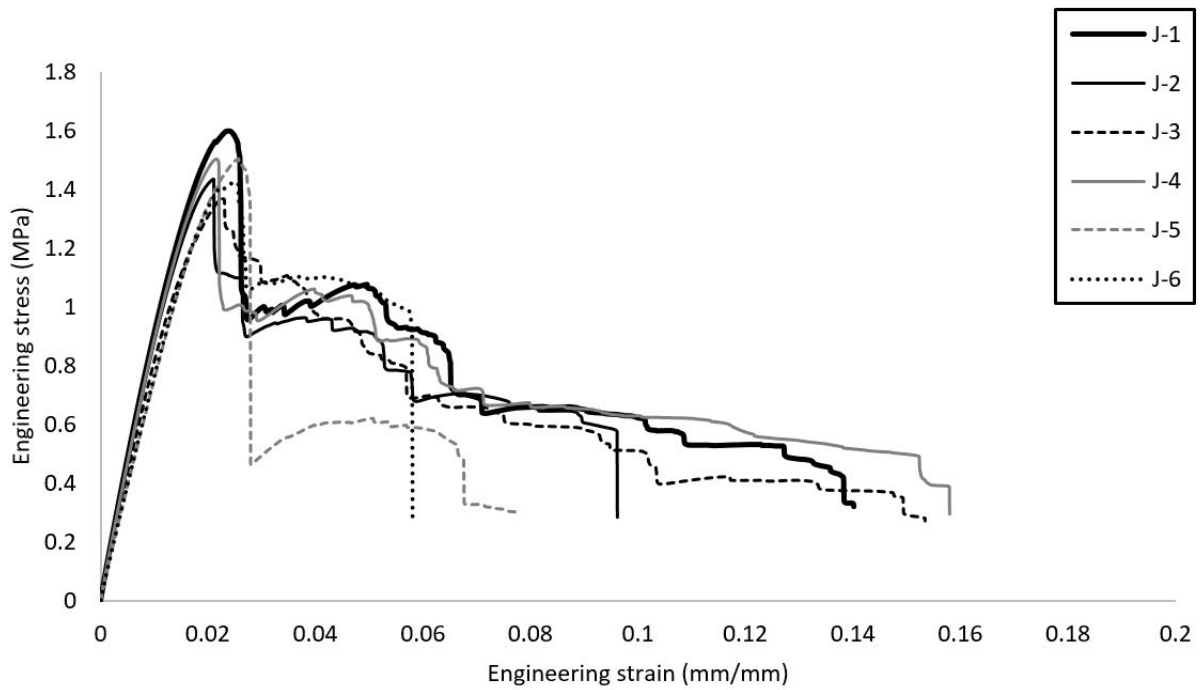
(d)
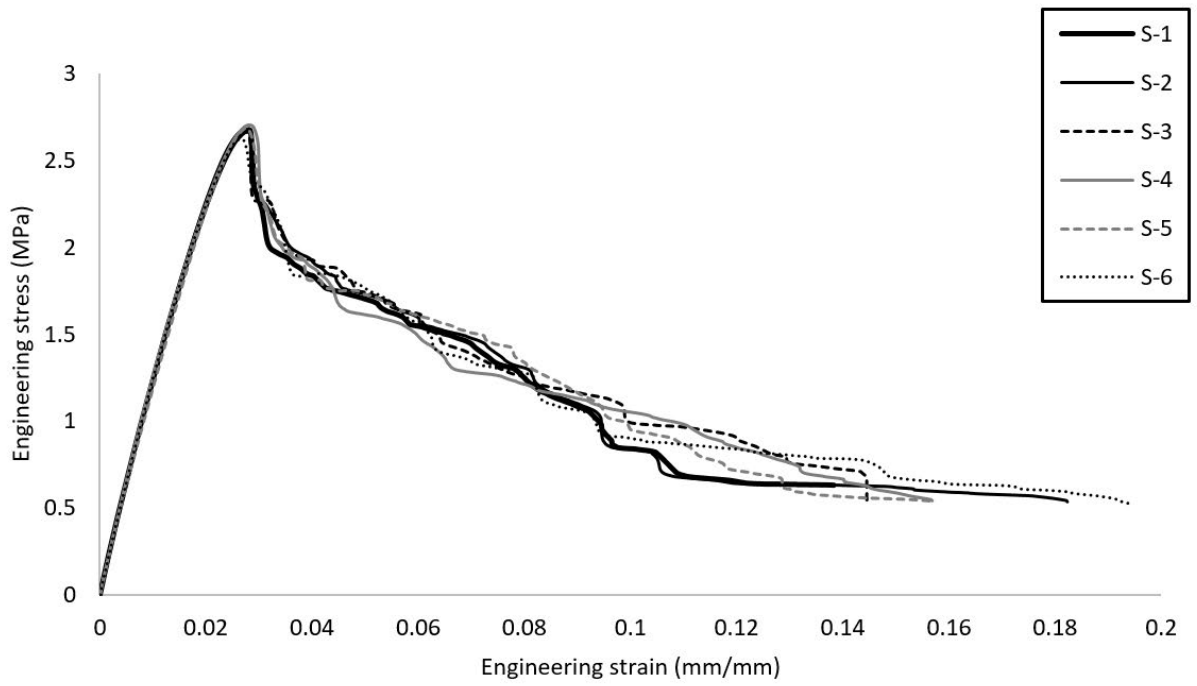
(e)
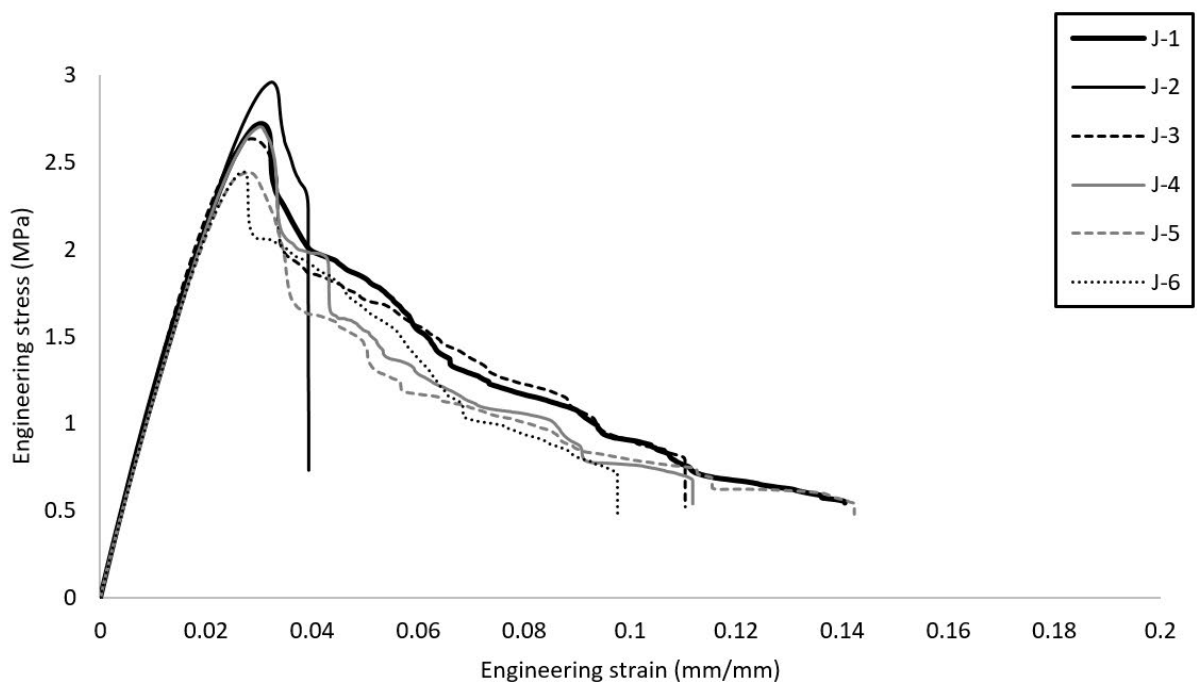
(f)
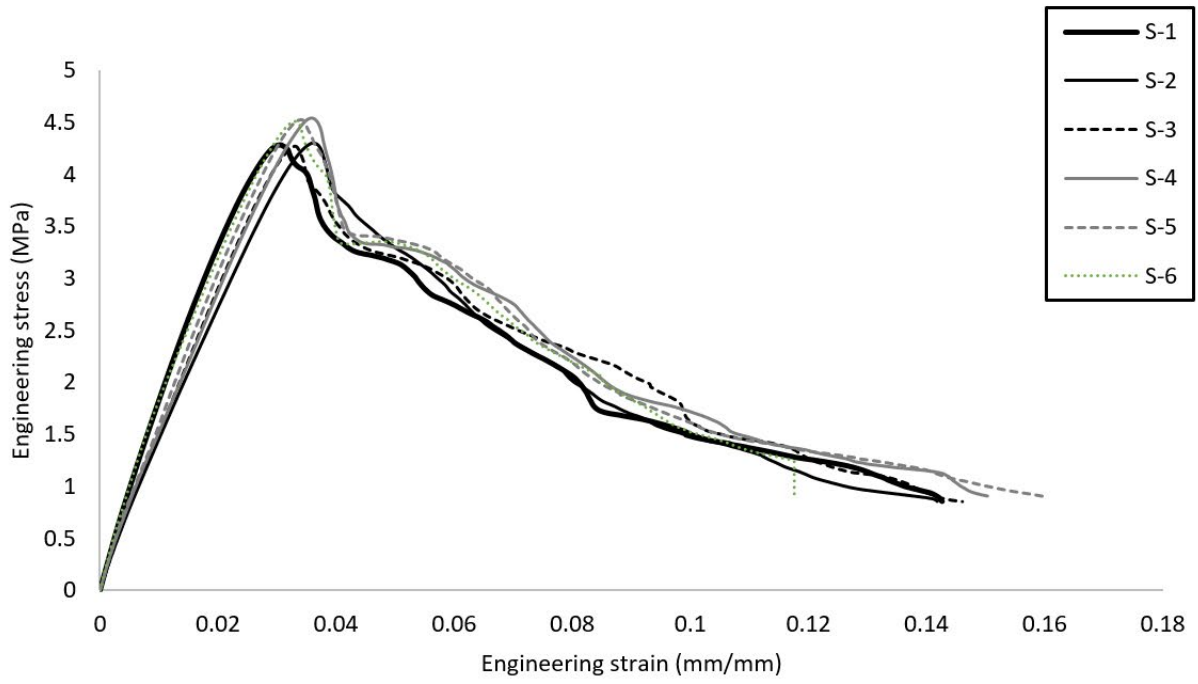
(g)
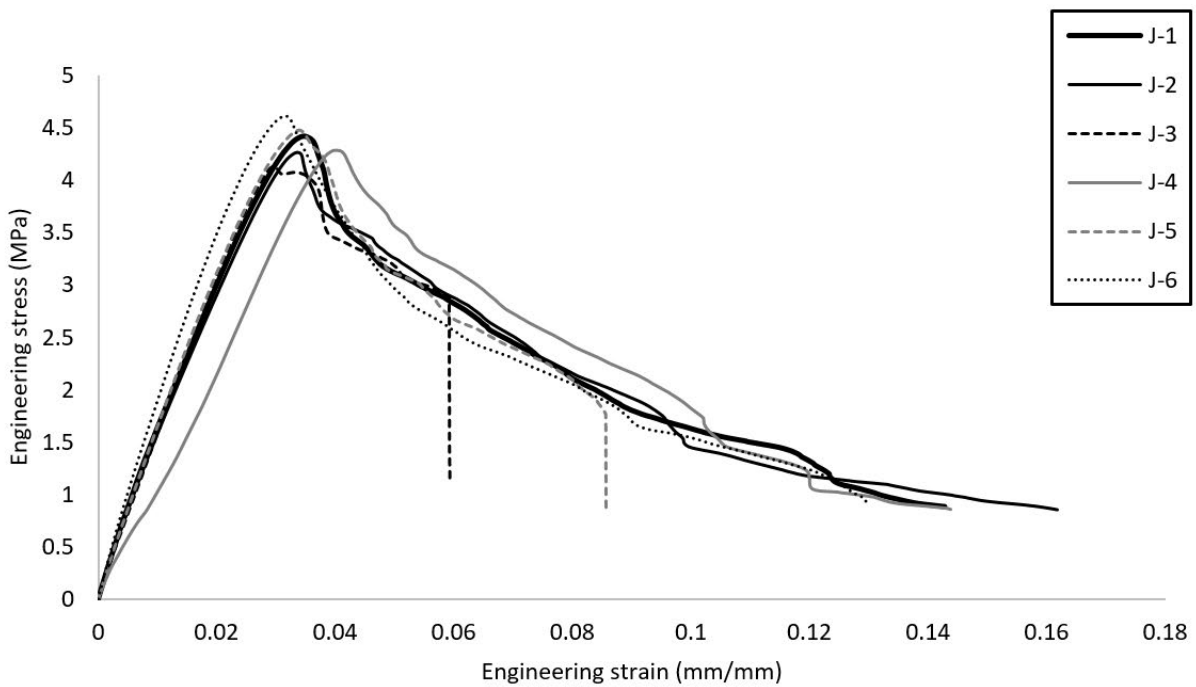
(h)

Fig. 16 Shear stress-strain curve with the corresponding images of deformation process: (a) standard specimen, d=1.0mm; (b) joined specimen, d=1.0mm; (c) standard specimen, d=1.5mm; (d) joined specimen, d=1.5mm; (e) standard specimen, d=2.0mm; (f) joined specimen, d=2.0mm; (g) standard specimen, d=2.5mm; (h) joined specimen, d=2.5mm.
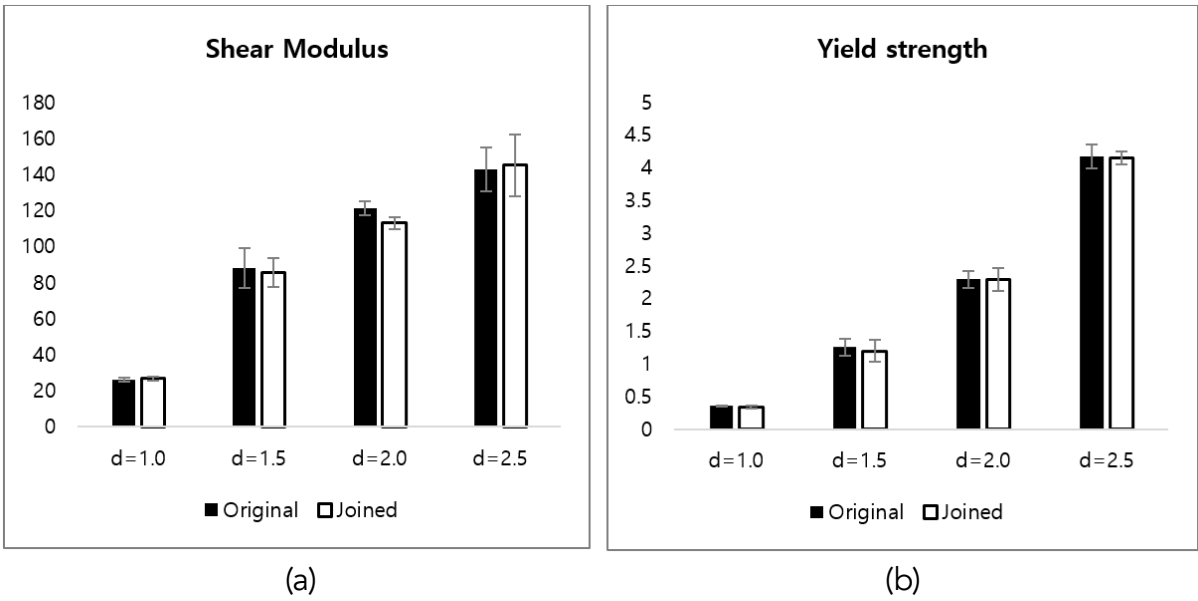
Fig. 17 Shear modulus and yield strength of both standard and joined specimens with four different strut diameters; (a) shear modulus and (b) yield strength.
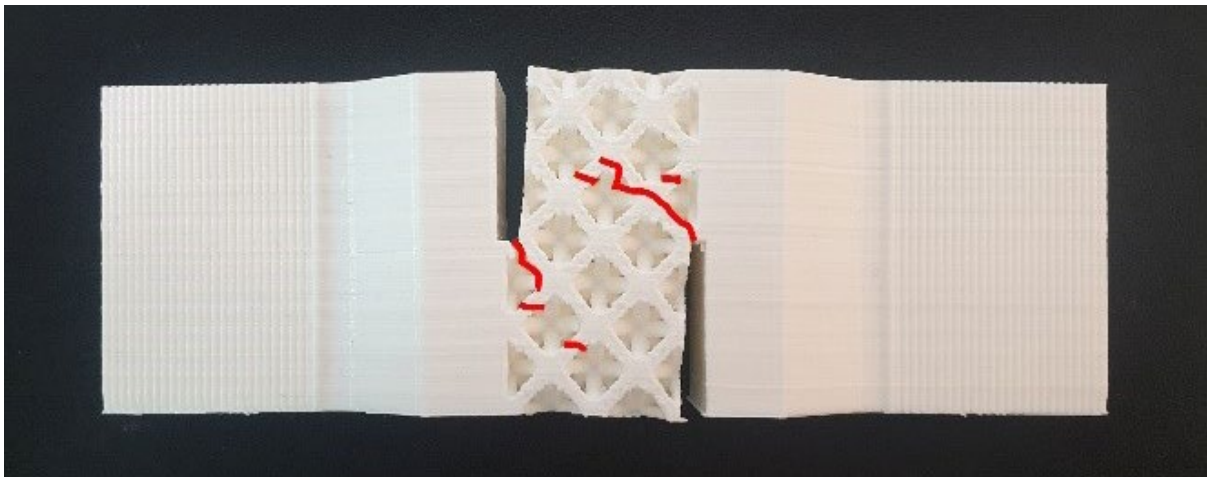
(a)
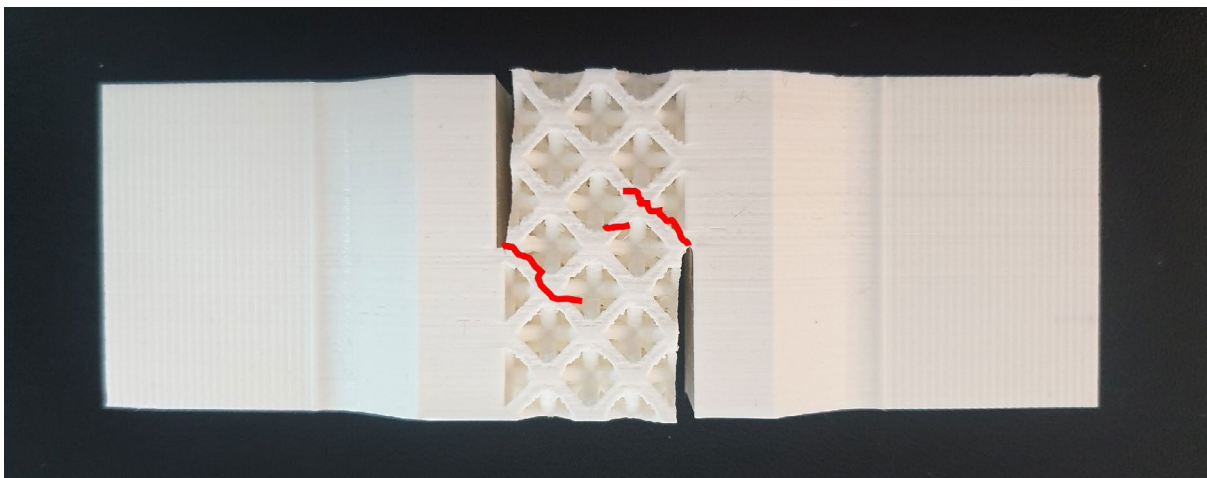
(b)

Fig. 18 Image of the specimens after shear test; (a) standard (d=2.0mm) and (b) joined (d=2.0mm).
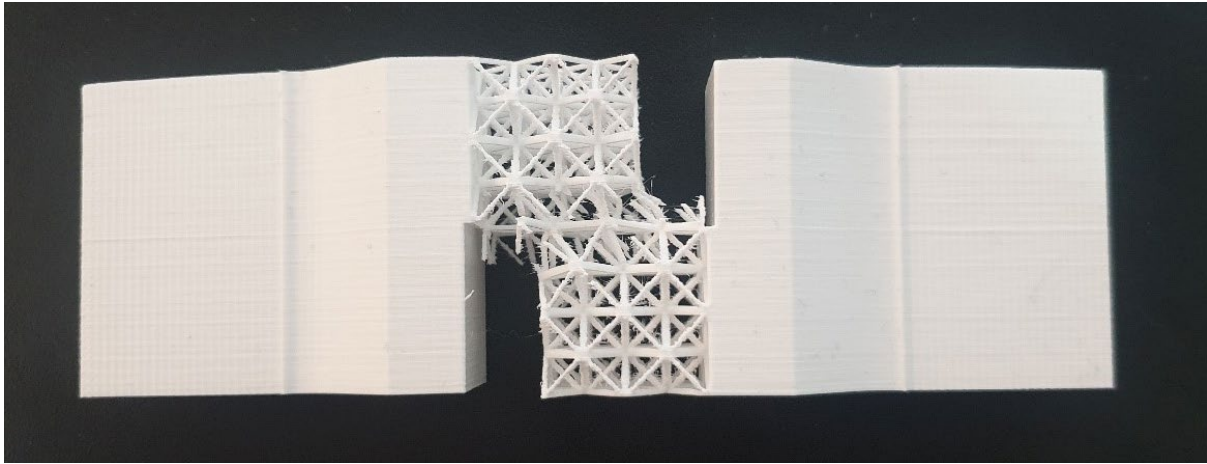
Fig. 19 Intertwined struts of lattice structure in the specimen with the diameter of 1.0mm after shear test.

3.4. Mechanical response of three-point bending

Similar to the tensile test results, the differences in the results between the two groups were evident (see Fig. 20(a)–(d)). When the strut diameter was 1.5 mm or more, the peak strength was significantly different between the two groups. In contrast, it was almost the same when the strut diameter was 1.0 mm.

Irrespective of the strut diameter, the stress increased again after the elastic response; this was caused by the deformation of the test specimens along with the buckling of the struts in contact with the loading pin. This tendency was more pronounced when the strut diameter was small. For a strut diameter of 1.0 mm, the specimen deformed layer by layer, resulting in a variation in stress as shown in Fig. 21. As the first layer of the specimen was loaded and deformed by the loading pin, the part (highlighted) next to the loading pin contacted the specimen and began to transmit the distributed load to the specimen, increasing the contact area. Thus, Fig. 20(a) shows the results up to the point where only the loading pin touches the specimen.

The test was stopped either when the specimen broke or when the adhesively bonded part failed before reaching the yield strength (Fig. 22), which was more prominent at larger strut diameters. When the strut diameter was 1.0 mm, the differences in appearance between the two groups were not distinct, but the standard specimens were more regularly deformed than the joined specimens, as shown in Fig. 20 (a). A few bonded struts of the joined specimens with a strut diameter of 1.5 mm were broken away before cohesive failure, but the specimens were also split into two parts in the end.

In general, as shown in Fig. 23, the mechanical properties of the joined specimens were lower than those of the standard specimens. However, the difference in flexural strength between the two groups was significant, while that of the flexural modulus was less significant.
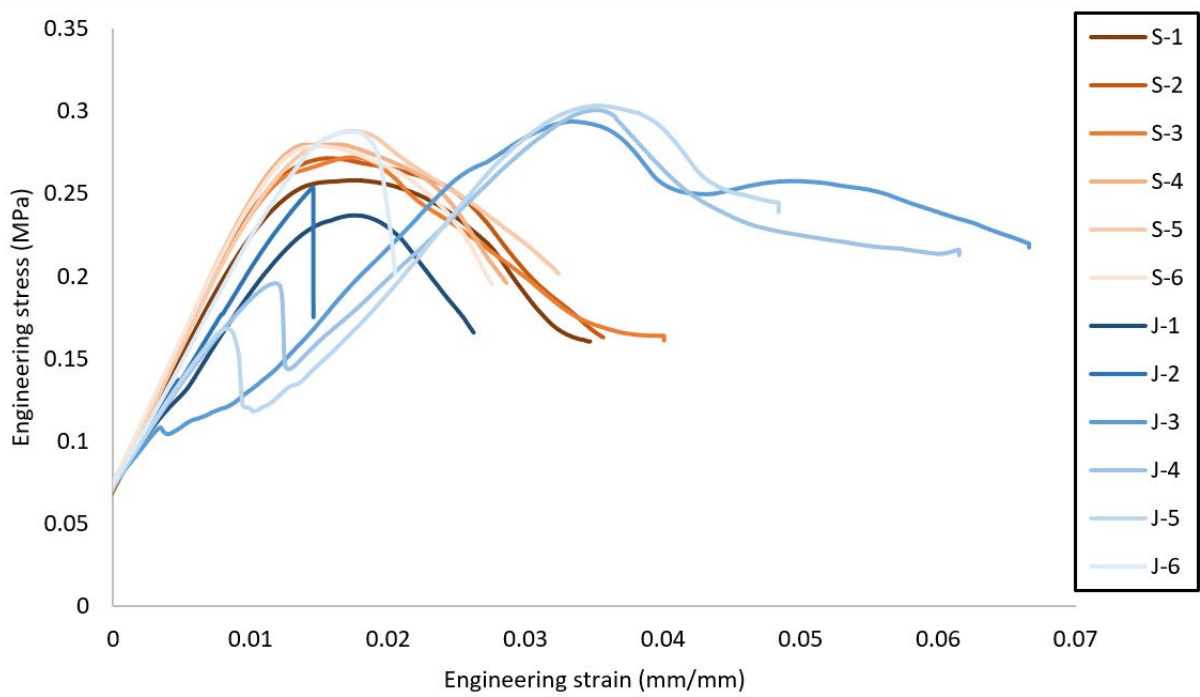
(a)
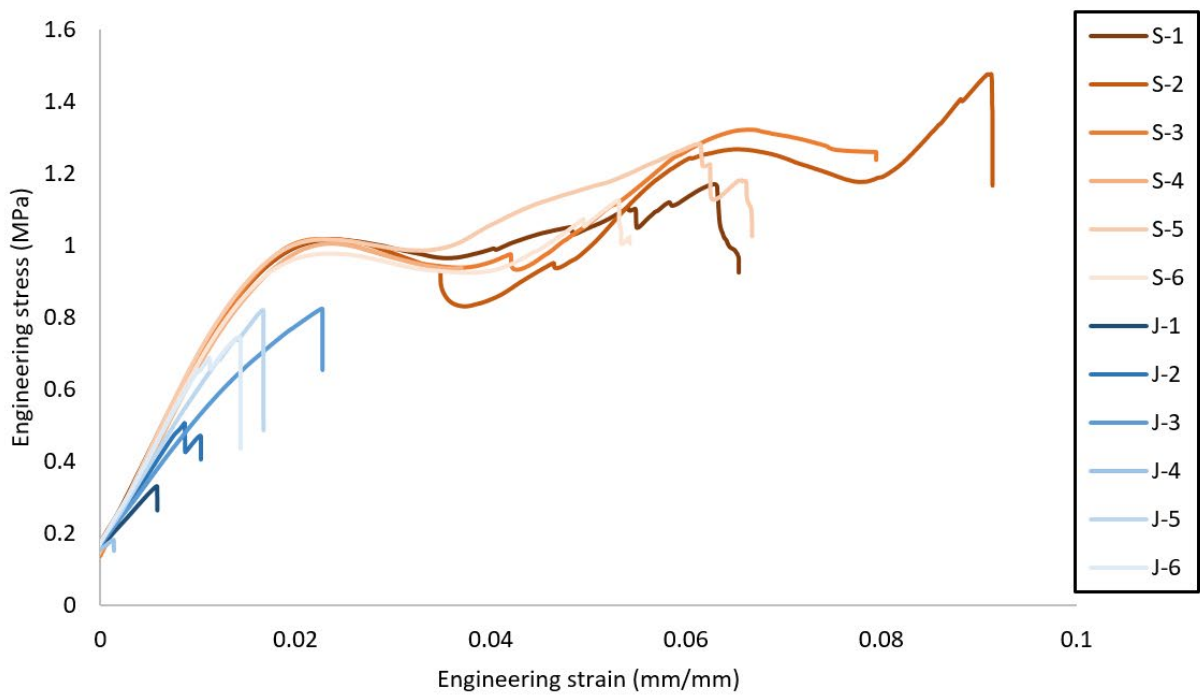
(b)
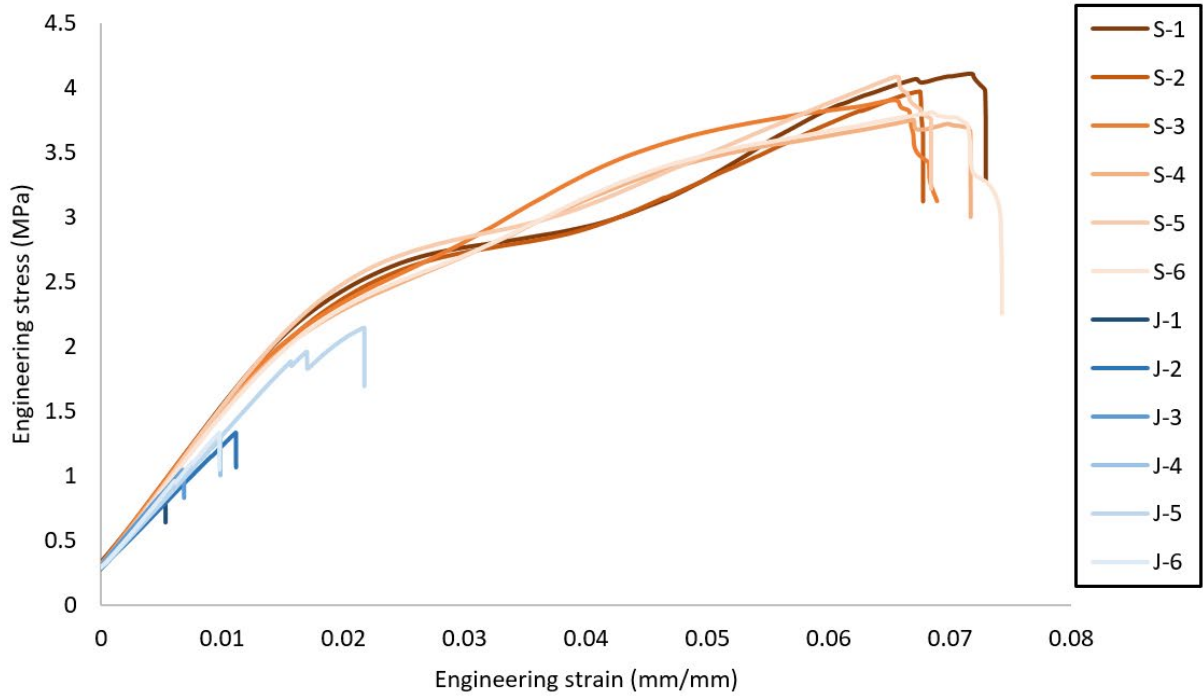
(c)
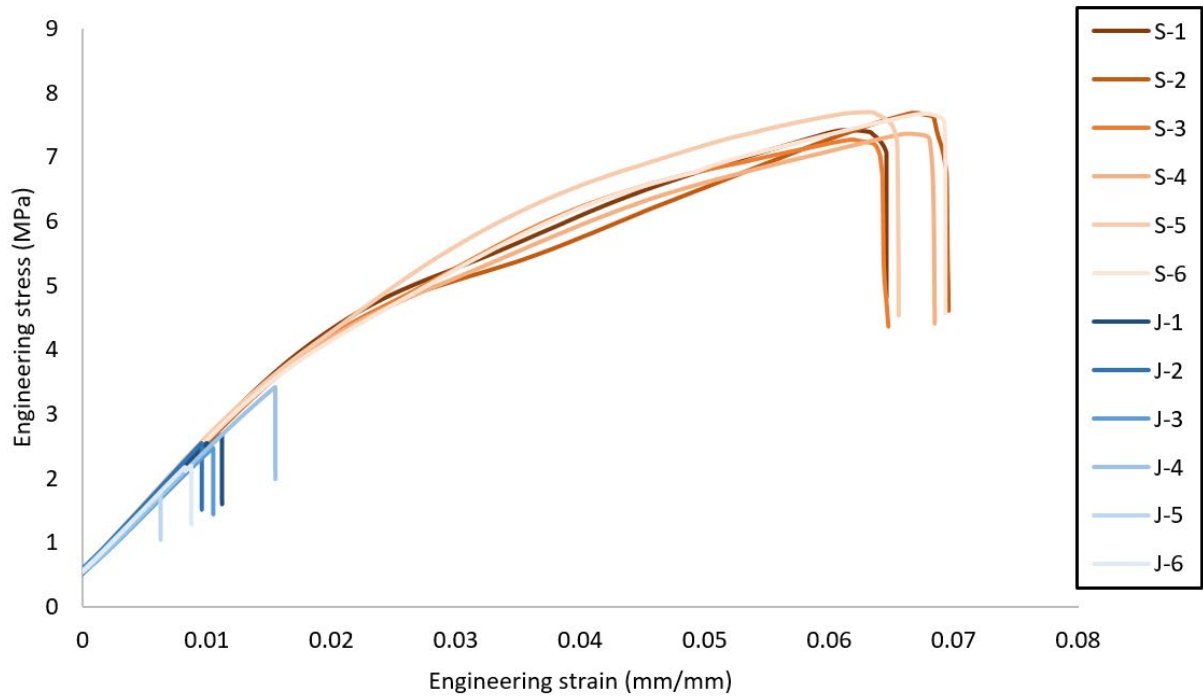
(d)

Fig. 20 Three-point bending stress-strain curve with the corresponding images of deformation process ('S' represents standard, 'J' represents joined): (a) standard and joined specimen, d=1.0mm; (b) standard and joined specimen, d=1.5mm; (c) standard and joined specimen, d=2.0mm; (d) standard and joined specimen, d=2.5mm.
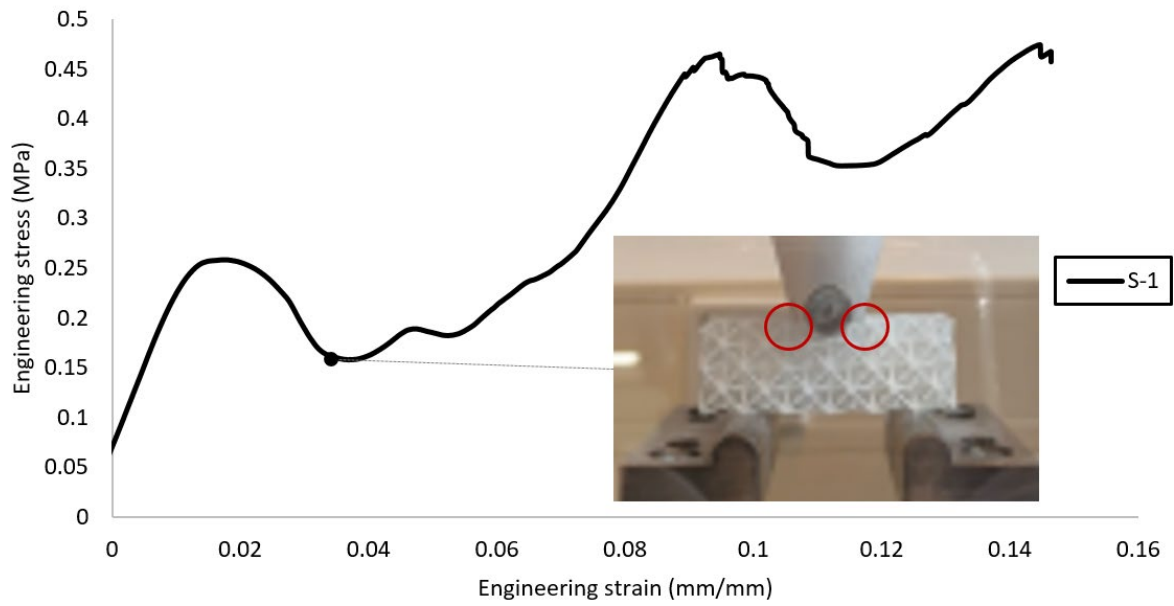
Fig. 21 Stress-strain curve extracted from three-point bending test with the standard sample with a strut diameter of 1.0mm. After the marked point on the curve, the holder located on both sides of the loading pin touched the sample and transfer the force, drawing the graph as shown above.

(a)   (b)
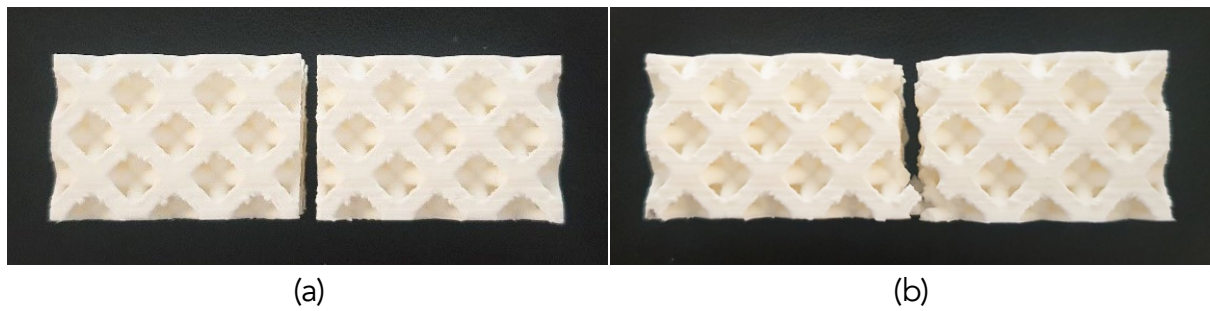
Fig. 22 Split samples after the three-point bending test with (a) standard (d=2.5mm) and (b) joined specimen (d=2.5mm).

(a)   (b)
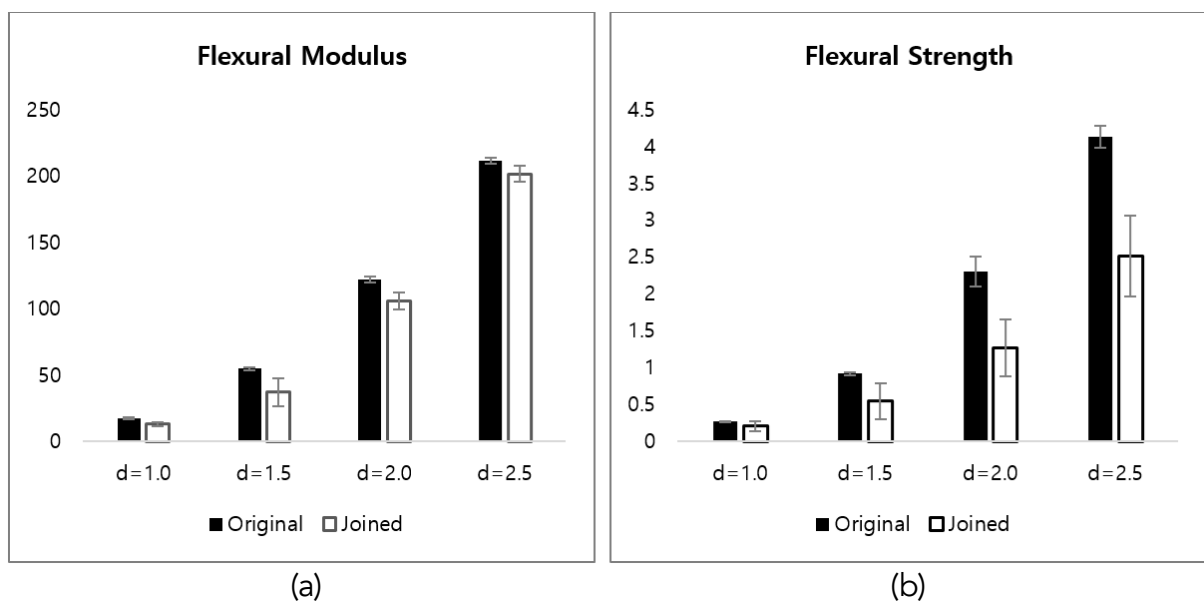
Fig. 23 Flexural modulus and yield strength of both standard and joined specimens with four different strut diameters; (a) flexural modulus and (b) yield strength.

4. Application

4.1. Application to the consumer products

   The data from the tests were applied to two types of door handles to create a guideline for repairing lattice structures. The lever type door handle (Fig. 24) had a cross section area of 2 mm × 2 mm of the lever part; it was made of the same type of unit cell and size used in the tests.

   Based on Fig. 24, the shear force diagram (SFD) and the bending moment diagram (BMD) are illustrated in Fig. 25.
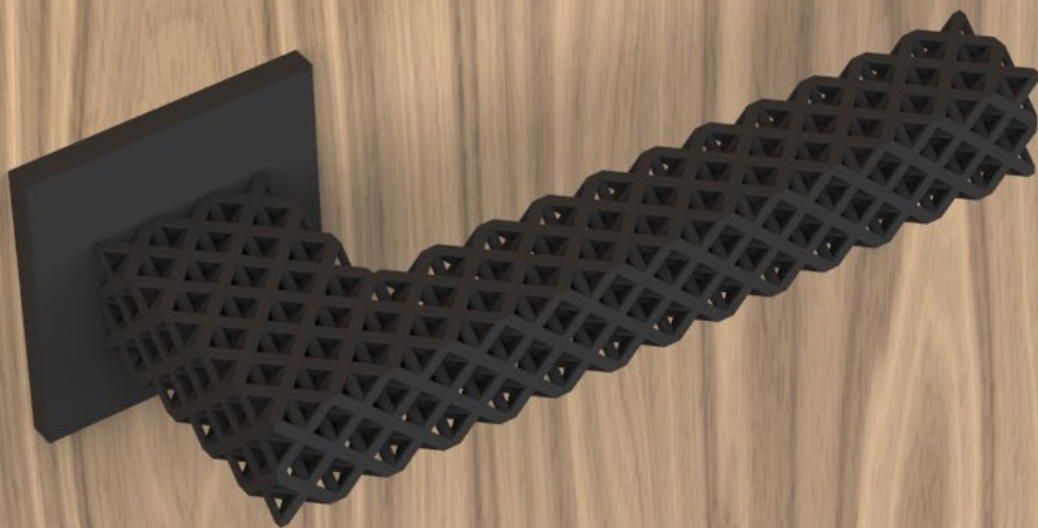
The lever type door handle rendered image

(a)

(b)
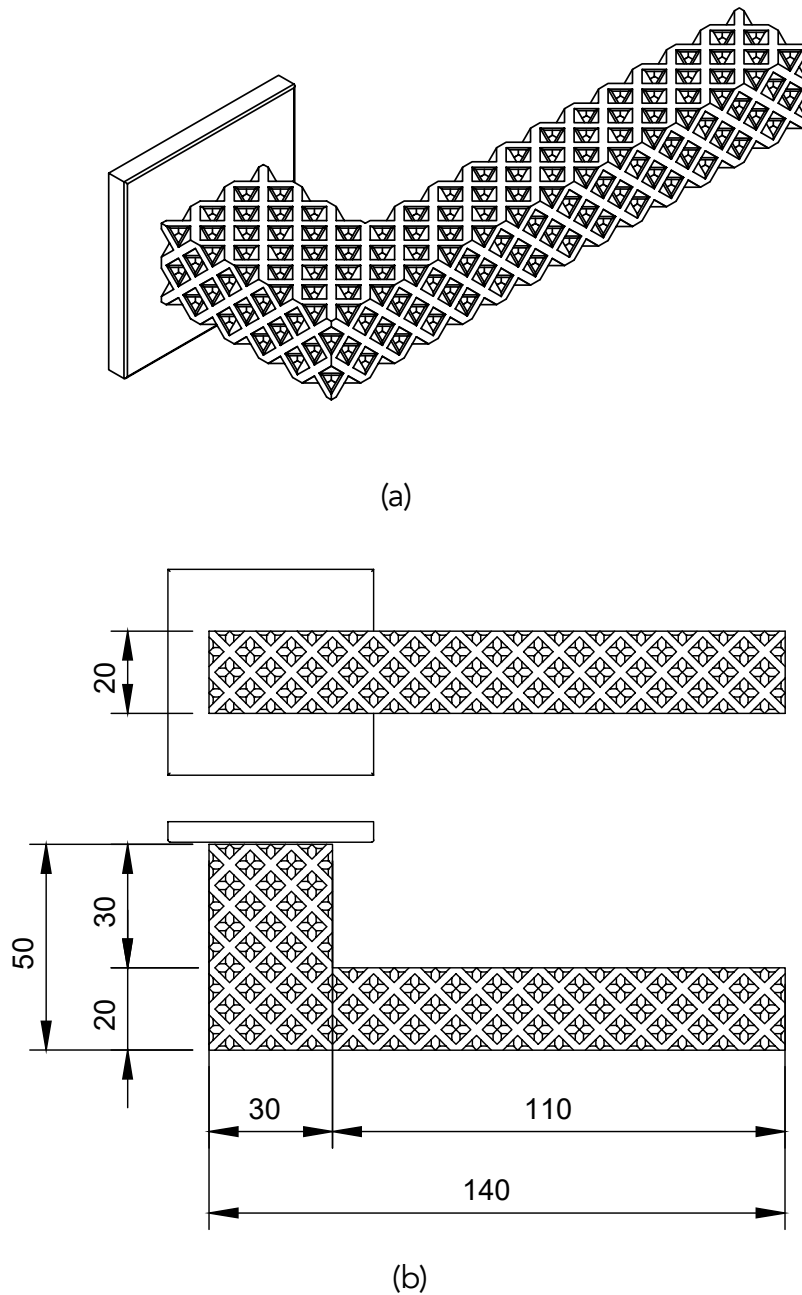
Fig 24 Schematic representation of the lever type handle: (a) perspective view; (b) front and top view.

The shear force calculation is as follows:

$\sum F_y = 0$; (y-axis)

$D_y = -0.1 \times 90 = 9\ Nmm$;

The bending moment calculation is as follows:

$\sum M_z = 0$; (anticlockwise: -)

$M_d = 0.1 \times 90 \times (15+45) = 540\ Nmm$;

$M_c = 0.1 \times 90 \times 45 = 405\ Nmm$;
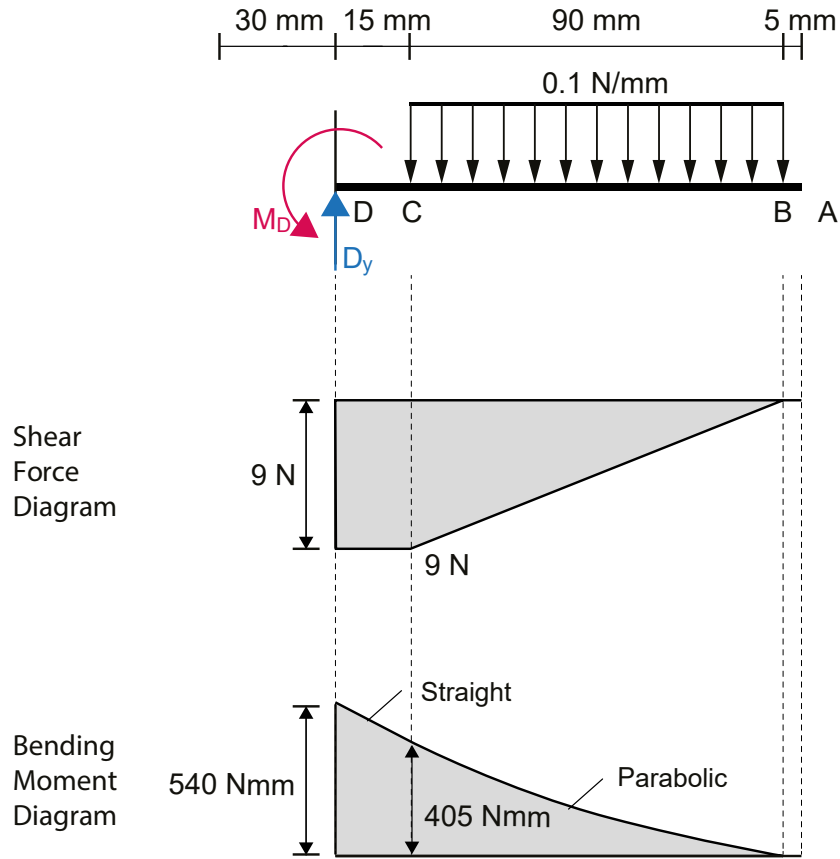
Fig. 25 SFD and BMD of the lever type door handle under the working stress.

As the bending stress is critical for joining two parts, and the shear stress was similar to the original state, the bending stress on the lever was calculated using the bending stress equation, Eq. (4), for the rectangular section.

$$\tau_b = \frac{Md}{2I} \tag{4}$$

where τ_b is the bending stress, M is the bending moment, d is the depth, and I is the moment of inertia, which was calculated using Eq. (5).

$$I = \frac{bd^3}{12} \tag{5}$$

where b is the width. Therefore, the maximum working stress was approximately 0.405 MPa. As the flexural strength of the standard specimen in the three-point bending test was 0.92±0.02 MPa when the strut diameter was 1.5 mm, the safety factor was approximately 2.27, which was determined by Eq. (6).

$$Safety\ factor = \frac{Yield\ strength}{Working\ stress} \tag{6}$$

However, the yield strength of the joined specimen was 0.54±0.25 MPa. The yellow highlighted region in the BMD in Fig. 26, which is the standard deviation of the yield strength, can be broken by the working stress if the repair on the handle is conducted in this region of the diagram.
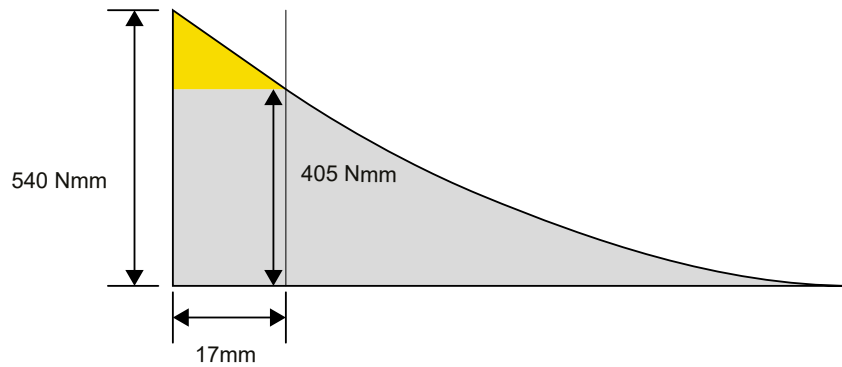
Fig. 26 BMD when the part is joined. The yellow area is within the yield strength under the safety factor of 1.
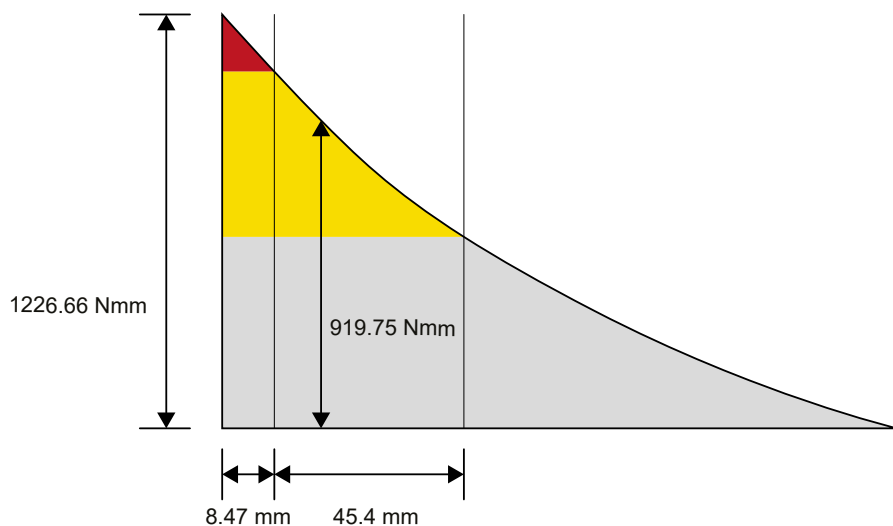
Fig. 27 BMD when the part is joined. The yellow area is within the yield strength and the red area is over the yield strength under the safety factor of 2.27, which is the same as the original product.

With a safety factor of 2.27, the BMD is drawn as shown in Fig. 27, where the red highlighted region in the diagram exceeds the yield strength, and the product can break when the force almost doubles. Fig. 28 shows the repairable area on the handle, where the green highlighted area can withstand the same yield strength as the original with a safety factor of 2.27.

However, if the parts are damaged in the red or yellow highlighted regions, they can no longer be repaired to achieve the same condition as the original. Using the torsional stress can be an alternative, as shown in Fig. 29, which induces a torque to produce shearing stress.

30mm

8.47 mm

45.4 mm

56.13 mm

Over the yield strength

Within the yield strength

Within the safety factor
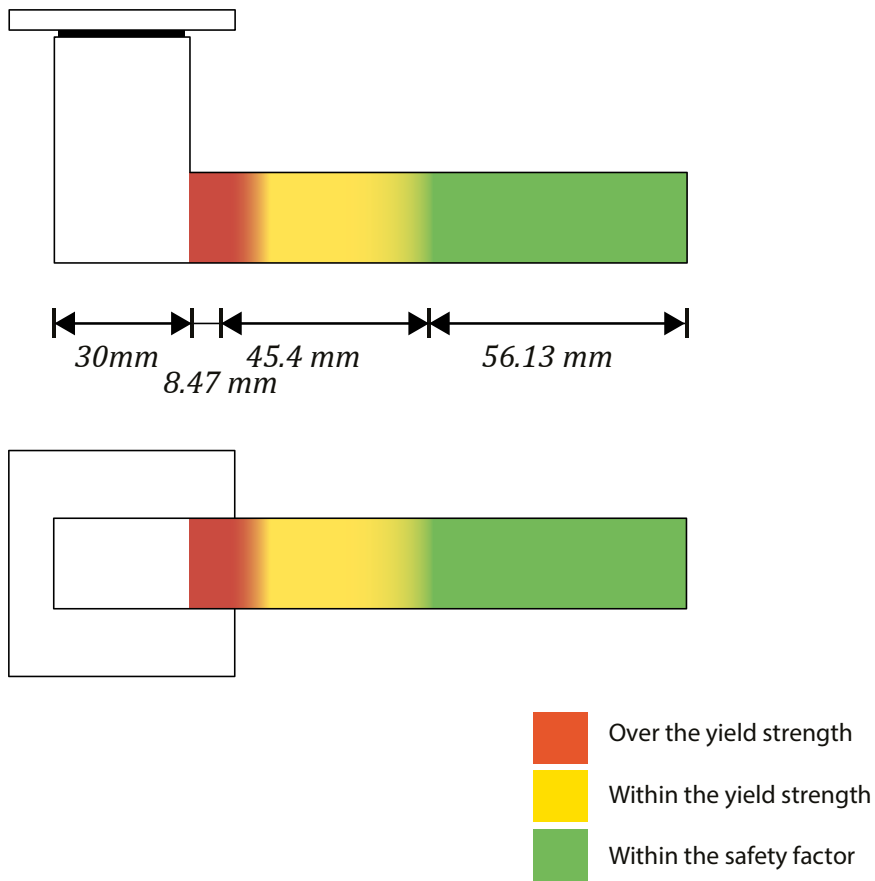
Fig. 28 Repairable area under the safety factor of 2.27. The green area indicates where the parts can be repaired as the same as the original.

Torsional shear stress
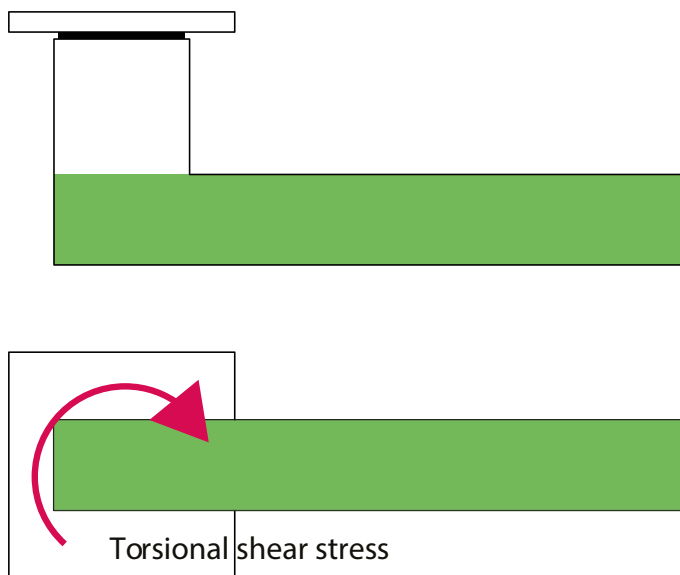
Fig. 29 Alternative way of repairing when the parts in the red or yellow areas are broken.

Fig. 30 shows the pull and push handle made of the same type and size of the unit cell as that of the lever, but with a strut diameter of 2.0 mm. The SFD and BMD are illustrated in Fig. 31 based on the effective span of the handle (see Fig. 32).

(a)   (b)
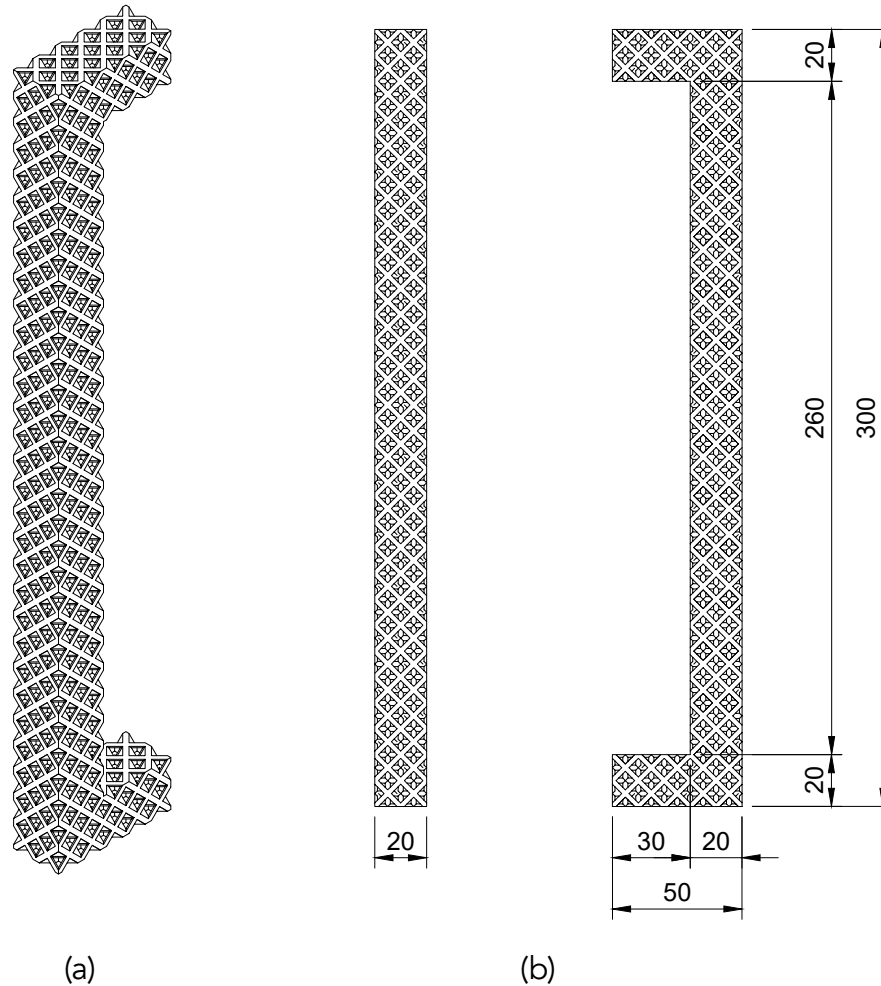
Fig. 30 Schematic representation of the pull and push type handle: (a) perspective view; (b) frond and side view.

The shear force calculation is as follows:

$\sum F_y = 0$; (y-axis)

$A_y = (90 \times 0.25(90+190))/(2 \times 280) = 11.25$ N;

$A_y = B_y = 11.25$ N;

The bending moment calculation is as follows:

$\sum M_z = 0$; (clockwise: +; anticlockwise: -)

$M_c = 95 \times 11.25 = 1068.75$ Nmm;

$M_{max} = (90 \times 0.25(2 \times 280-90))/8 = 1321.88$ Nmm;
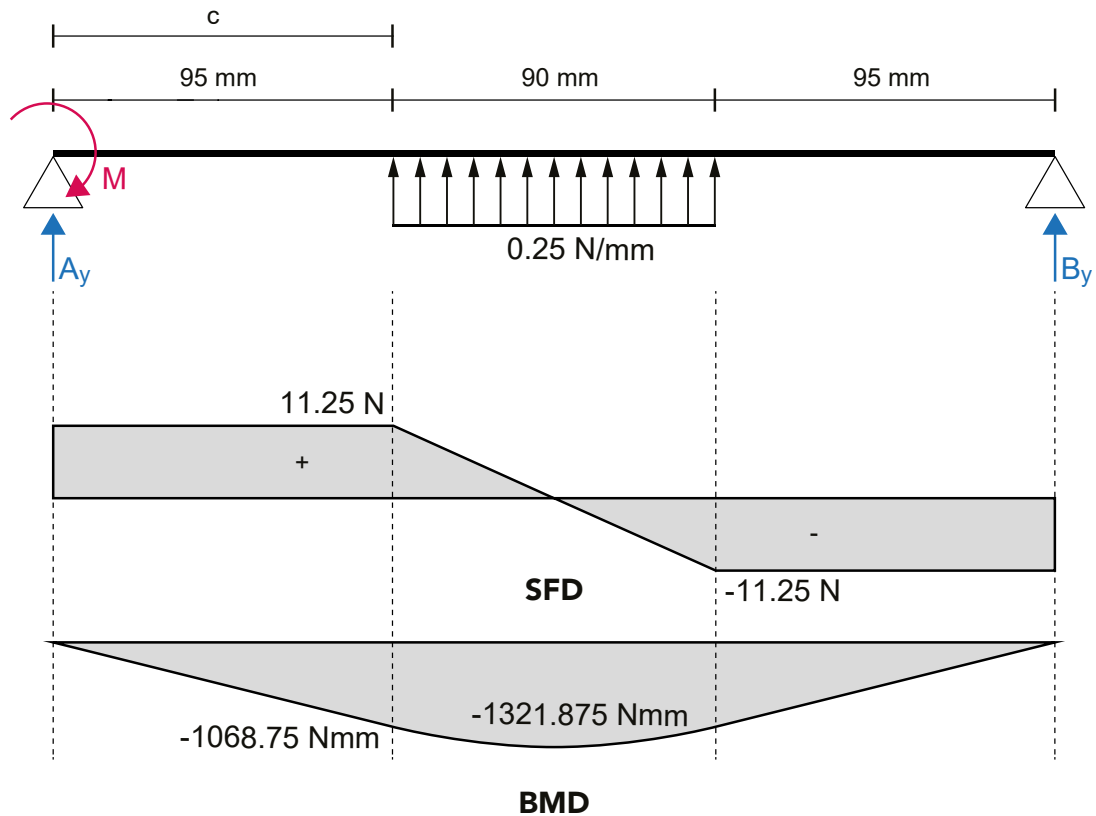
Fig. 31 SFD and BMD of the pull and push type door handle under the working stress.
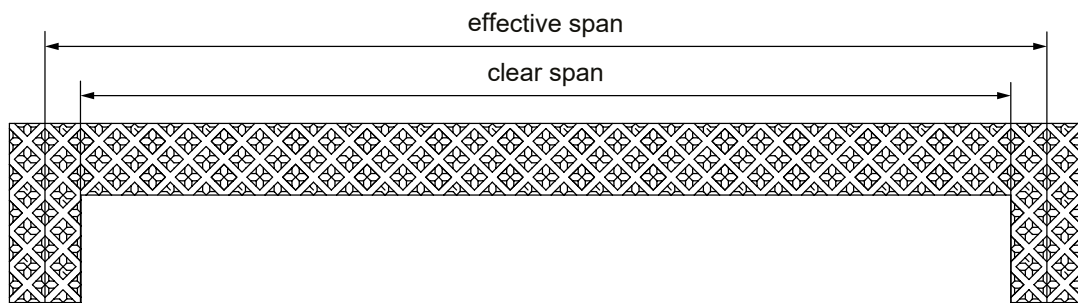
Fig. 32 Spans in simply supported beam.

As the flexural strength of the standard specimen was 2.3±0.2 MPa when the strut diameter was 2.0 mm, the safety factor of the pull and push handle was approximately 2.32. However, when the handle was adhesively bonded, its middle part became unrepairable under the same safety factor as the original, as shown in Fig. 33. Fig. 34 shows the repairable area on the handle. As long as the products are repaired in the green area, they can have the same safety factor as the original product. However, the red and yellow regions account for a relatively high proportion, as observed in Fig. 34, which leads to a wastage of printing time and material if only a

small part of the surface of the product is damaged. Such cases can be addressed by repairing the damaged part of the unit cell layer of the product, thus producing compressive stress, as shown in Fig. 35.
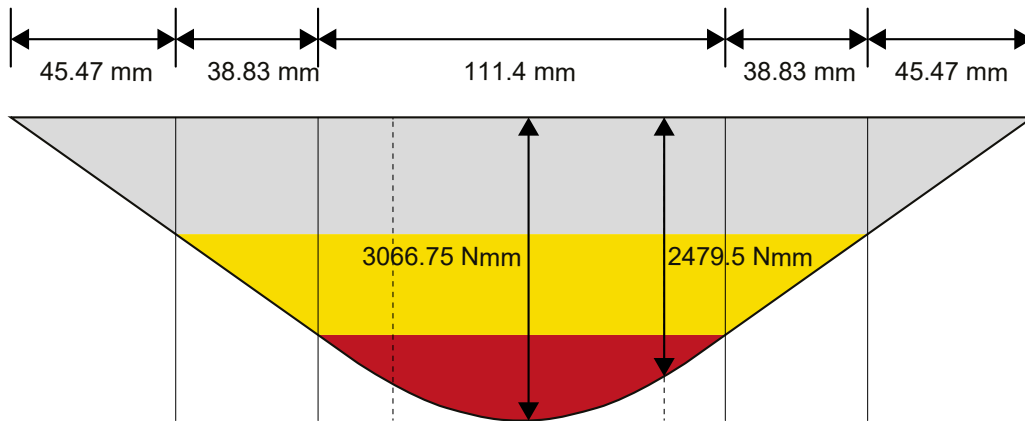
Fig. 33 BMD when the part is joined under the safety factor of 2.32, which is the same as the original product.
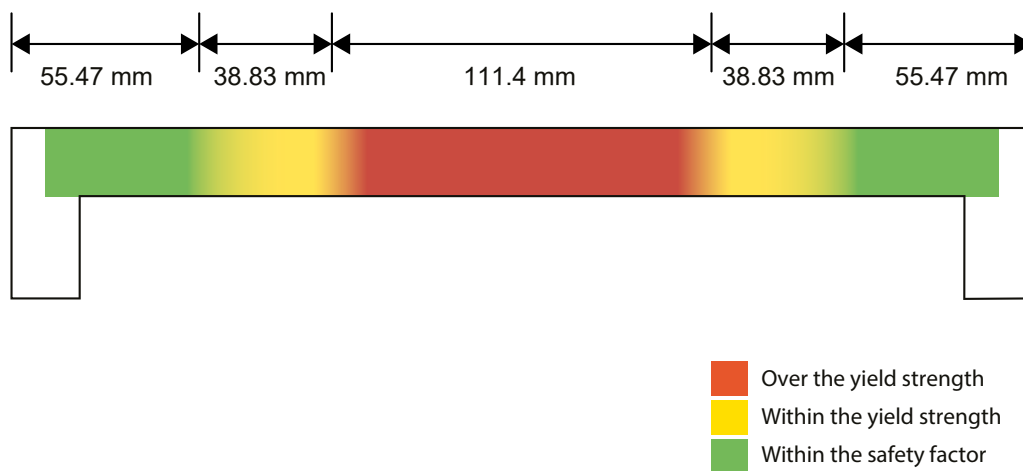
Fig. 34 Repairable area under the safety factor of 2.32. The green area indicates where the parts can be repaired as the same as the original.
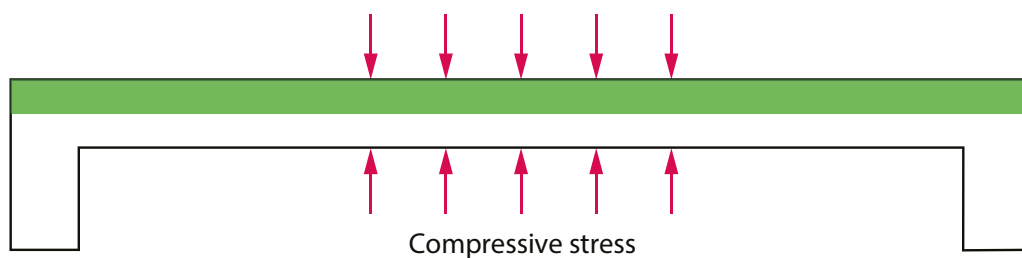
Fig. 35 Alternative way of repairing in order to make compressive stress instead of bending stress when the surface of product is damaged in the red or yellow areas.

The pull & push door handle rendered image.

4.2. Repairing the lattice structure in the circular economy model
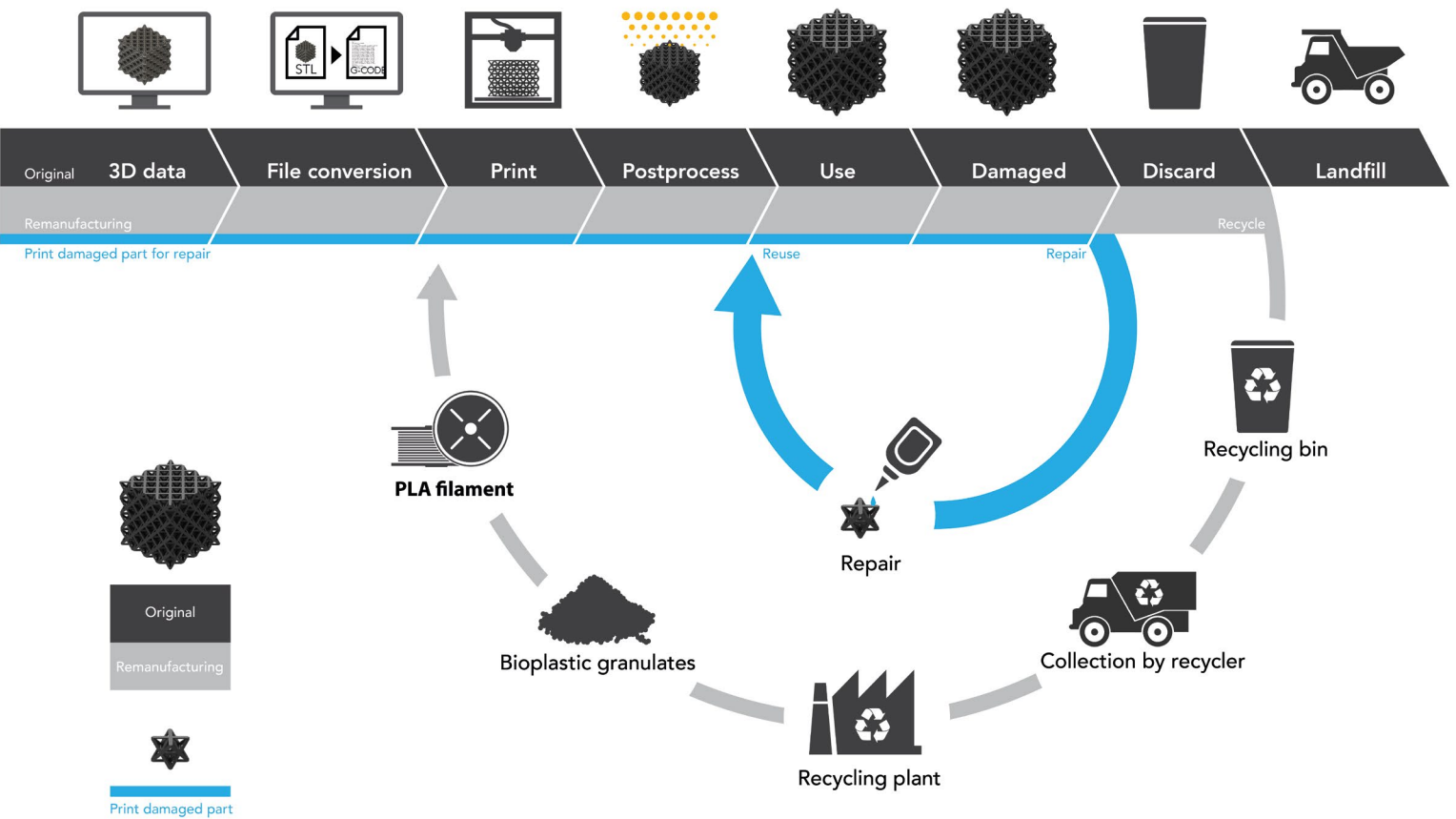
Fig. 36 The flow of repair of the additively manufactured lattice structure adapted from Fig. 2 and the circular economy model by Ellen MacArthur Foundation.

Fig. 36, which is adapted based on Fig. 2 and the circular economy model developed by the Ellen MacArthur Foundation (3), shows the flow of products with lattice structures when users design their own products for their intended objective and produce them using FDM with PLA. Here, the black linear flow represents the manufacturing of the original products, the grey large circular flow is remanufactured through recycling, and the small blue circular flow is reused through repair in the circular economy. In the flow of repairing, the need to fabricate the same size and shape as the original part for the damaged position may not seem significantly different from the remanufacturing process. However, a more complex or large structure requires more material and time to produce, which plays a major role in the economic value of AM (23, 54). In addition, the ability to print the necessary part is an advantage of AM technology as it is capable of mass customisation.

In terms of the recycling of biodegradable PLA, with the development of chemical

recycling, there have been many improvements in the economic value (55). Nevertheless, resources are still required in the processes of collecting, transporting, sorting, and processing, which release CO_2 (12).

For the design of lattice structures, the mechanical properties are often determined for the intended objectives(56-58), hence the model assumes that users would design the structure themselves. However, owing to the nature of AM technology, the production and consumption of lattice structures can be diverse (4), resulting in slight changes in the flow in the model. However, in all cases, the repair and maintenance of the lattice structure has a beneficial impact on the environment in a circular economy.
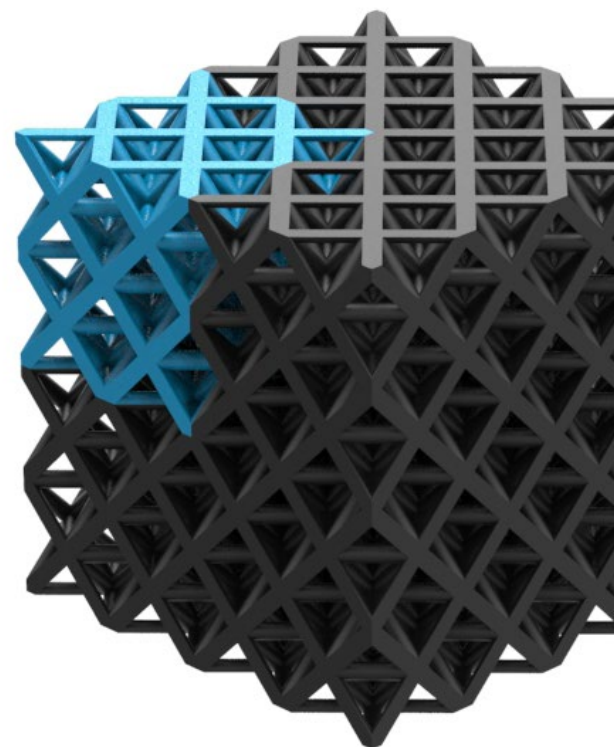
5. Discussion

In this study, FDM and PLA, which are relatively competitive with respect to price and availability, were selected as the production method and material, respectively. A total of 198 specimens were used for the test, including solid specimens used in compression and tensile tests: compression (n = 48 + 8(solid)), tensile (n = 48 + 8(solid)), shear (n = 48), and three-point bending (n=48).

The results showed a similar mechanical response when the damaged parts were repaired using compressive or shear stress direction, satisfying the LoR. However, the use of tensile strength and flexural strength showed a considerable difference in mechanical response after repair. The appearance after repair was less marked and similar to the original state when the parts were bonded in the printing direction, but the bonding direction was not controllable because it was determined by the location of failure.

The lattice structure used in this study was limited to a periodic array, allowing the damaged parts to be accurately measured on a unit-cell basis. This feature also made it easier to reprint and reassemble the required parts. However, studies on the trimming methods of damaged parts have not been conducted independently; hence, further studies are required to evaluate the comprehensive repairability of lattice structures.

The data used in this study was easy to access and edit because it was created by us. Accordingly, irrespective of the process of data creation and consumption, it should be accessible and editable for repair, as access to editable data is essential for repairability.

5.1. Limitations in application

For the application, simplified diagrams were drawn based on actual measurements. The amount of reaction force and the distributed force may vary depending on the type and material of the handle, the size of the hand, and the location of the grip.

Specific values of yield strength from the test were directly used to compare the yield strength of the specimen products as the specimens had the same thickness and depth as the test specimens. However, not all the exact values of the mechanical responses for all variables can be known. Thus, the test results may be applied in the form of the procedure detailed in Section 4.1 for the repair of the lattice structure, but it may be difficult to produce such accurate guidelines.

The mechanical response under torsion shear stress may be different from that under the direct shear test. Therefore, an additional adhesive test with the lattice structure is necessary to validate the assumption of the application. Furthermore,

the joint design for enhancing the joint strength has been investigated (59, 60), which seems to be suitable for joining lattice structures in the form of a double butt joint, stepped joint, tongue and groove butt joint, recessed double strap joint, etc. (see Fig. 37). Hence, different joints can address the limitations in tensile and three-point bending stresses.

(a)   (b)   (c)   (d)
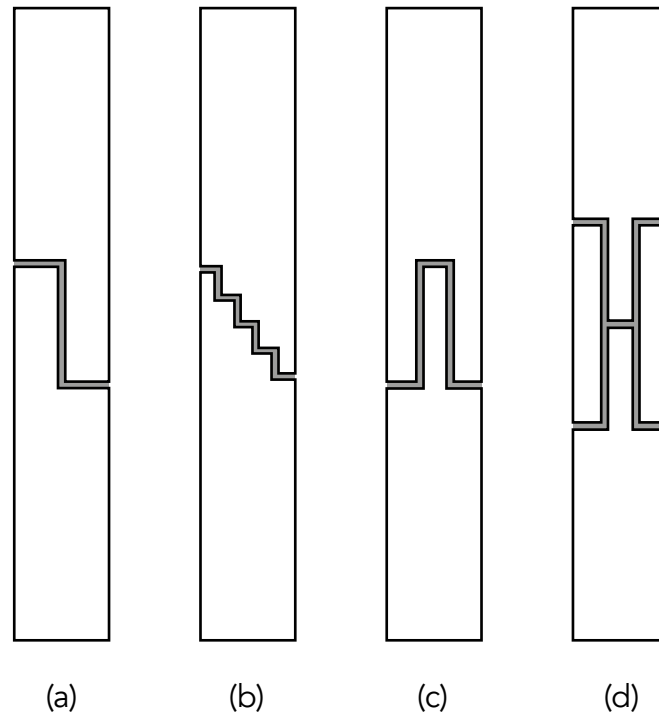
Fig. 37 Examples of joint methods that showed the better result under tensile and bending stress in the previous study (1); (a) double butt joint, (b) stepped joint, (c) tongue and groove butt joint, and (d) recessed double strap joint.

5.2. Effects of test parameters

The specimens for pilot testing were fabricated with PLA using the same printing parameters on two 3D printers, Ultimaker 2+, but the results showed that the mechanical responses differed considerably depending on the printer and material, as shown in Fig. 37. The PLA used in the pilot test was the same white PLA manufactured by the same company, but on different days and years. S-P1-M1 (Fig. 38) was more brittle, while the others were ductile, tearing in the direction of the printed layer. The specimens were all white coloured, but differed slightly. Therefore, it is important to realize that differences in mechanical responses, which may occur depending on the printer or material, can be greater than the differences between the original and the repaired lattice structures.
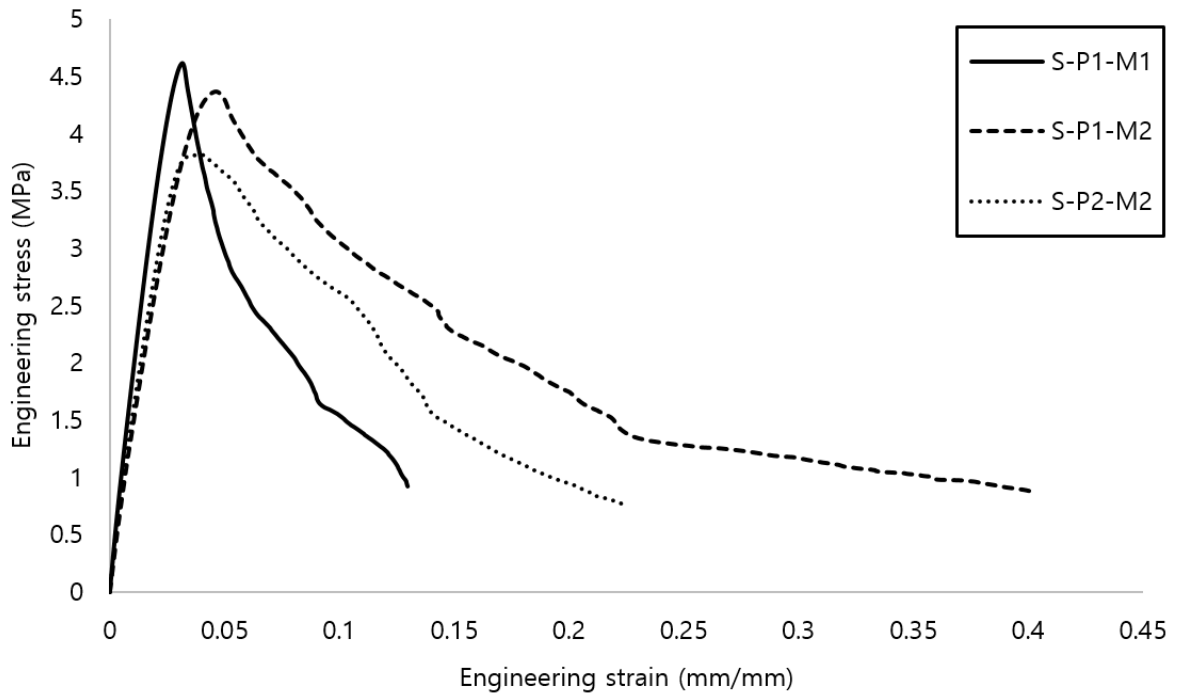
Fig. 38 Mechanical response of the specimens printed in different printer with different PLA; (a) stress-strain curves from the shear test tested by specimens with three different parameters ('S' represents standard specimen, 'P' represents printer, 'M' represents material), (b) specimens after the shear test.

5.3. Recommendations

The material along with the geometry and relative density determine the properties of the lattice structure (61). Selecting the appropriate adhesive is also crucial as the adhesion strength of the adhesive is associated with the adherends (52). Moreover, properly trimmed surfaces influence the adhesion strength (52). Hence, I trimmed the surfaces of the joined specimens for the tensile and three-point bending tests before testing in order to improve the adhesion strength. This is because the joined specimens for the pilot test, which had not been trimmed, showed almost half the yield strength of the standard specimen. However, as observed in Fig. 39, the adhesion did not increase noticeably regardless of whether the surface was trimmed because all the joined specimens showed cohesion failure not only for the main test but also for the pilot tests with other adhesives (Fig. 40) in the tensile and three-point bending tests. Thus, trimming the surface is not necessary subject to further tests being set in the same condition; however, the cohesive strength needs to be considered for the selection of the adhesive.

All the processes proposed and conducted in this study may be used as references or guidelines for future experiments using different materials or geometries.
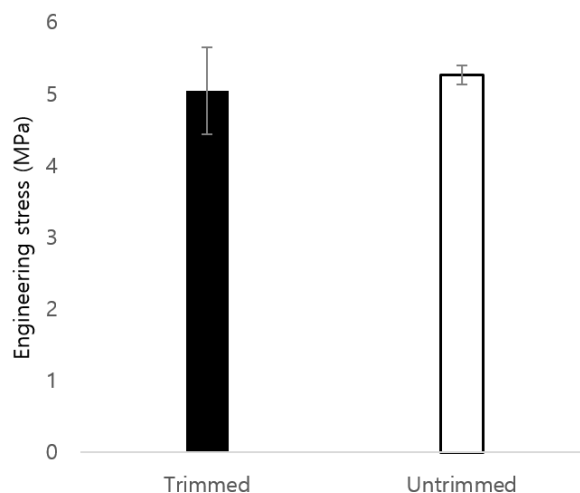
Fig. 39 Compare of mechanical response between trimmed and untrimmed specimen.

| (a) | (b) | (c) |
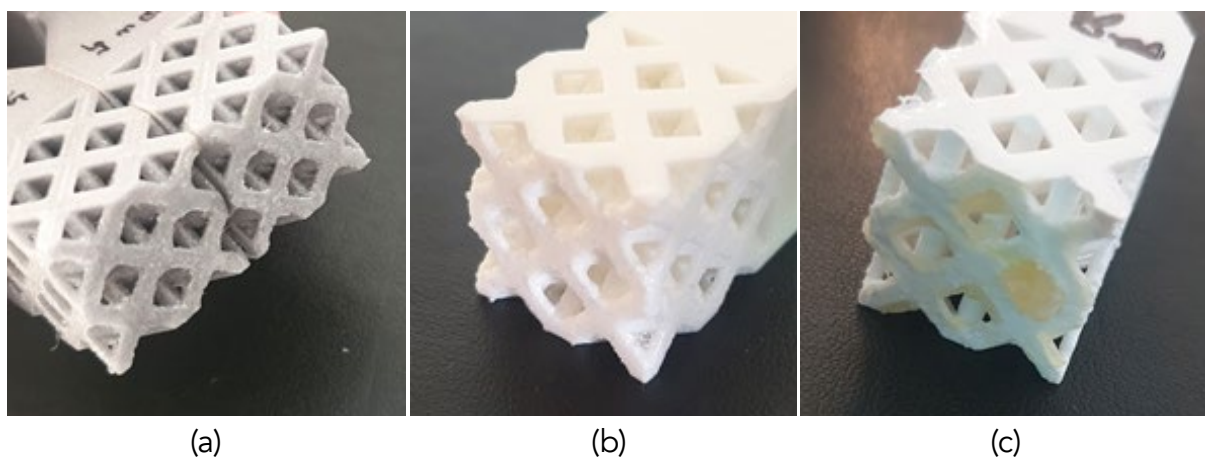
Fig. 40 Cohesive failure in the tensile test; (a) plastic glue, (b) PVC cement, (c) epoxy.

6. Conclusions

In this study, the important factors that need to be considered in repairing lattice structures were investigated so as to enable reusing of lattice-structured products and get people involved in extending the lifespan of the products for the circular economy. The octet-truss lattice specimens with four different strut diameters in each standard and joined group were tested under quasi-static loading: compression, tensile, shear, and three-point bending tests. The specimens were fabricated using FDM with PLA. In each test, the mechanical responses of the standard and joined specimens were compared, and the deformation of all the specimens was examined during and after the test. The key findings of the test results are as follows:

- The difference between the mechanical behaviour of the joined and the standard specimens with respect to the compressive stress is not significant. However, as the strut diameter increases, the joined specimens show a plateau section in the plastic region and deform uniformly, reducing the shock absorption capability.

- Both standard and joined specimens exhibit remarkably similar shear responses, although the deviations for the joined specimens are slightly larger due to adhesion, which can be affected by various factors.

- For all the tests, the young's modulus of the joined specimens show marginally lower values as compared to that of the standard specimens, but most of these values are within the standard deviation.

- The yield strengths of the two groups differ considerably in the tensile and three-point bending tests, which is clearly evident when the lattice structure is stronger than the adhesive force as the strut diameter is increased. In contrast, the difference in yield strengths between the two groups is not significant in the compression and the shear test.

To summarise, it is crucial to consider the direction of stress as well as the selection of adhesives for repairing 3D printed octet-truss lattice structures. With proper guidelines for the repair of the lattice structures, a more efficient flow can be created for managing resources in a circular economy, thereby minimising the environmental impact.

Appendix A

List of requirements

The list below is requirements of the lattice structure for the study.

Req. Id	Priority	Requirement description
Req. 1	Low	**Manufacturing** The structure should be manufactured by AM
Req. 2	Low	**Manufacturing** The lattice structure should be mesoscale
Req. 3	Low	**Manufacturing** The dimension of each unit cell should be between 2mm to 50.0mm
Req. 4	Low	**Manufacturing** The maximum size of the array should be less than 250 X 210 X 210
Req. 5	Low	**Performance** The structure should be stretch-dominated
Req. 6	High	**Performance** The lattice structure should have the same or similar properties after repairing the damaged parts
Req. 7	Medium	**Performance** The lattice structure should look the same or similar appearance after repairing the damaged parts
Req. 8	Low	**Performance** The structure should satisfy the desired functionality of the consumer product
Req. 9	High	**Repairability** The shape of the damaged part for reproduction should be identified accurately
Req. 10	High	**Repairability** Data for reproduction of the damaged parts should be made easily or highly accessible
Req. 11	High	**Repairability** The damaged parts should be printed by 3D printer
Req. 12	High	**Repairability** Re-assembly of printed parts should be convenient
Req. 13	Low	**Repairability** The structure should be recyclable after replacement of the part

Appendix B

Adhesive selection test

Before the main test, compression, tensile, and shear test were carried out in order to select the most suitable adhesive that can show similar mechanical properties and appearance to the original. The six types of adhesives were selected based on the specification of the adhesives: cyanoacrylate, plastic glue, silicone glue, epoxy, acetone, and PVC cement. However, since the specimens glued by acetone and silicone fell off comparatively easily, they are excluded from the tests. For the test, the same specimen design was used with the diameter of 2.5mm, which strut are the stiffest. Fig. B1 show the results of three tests.
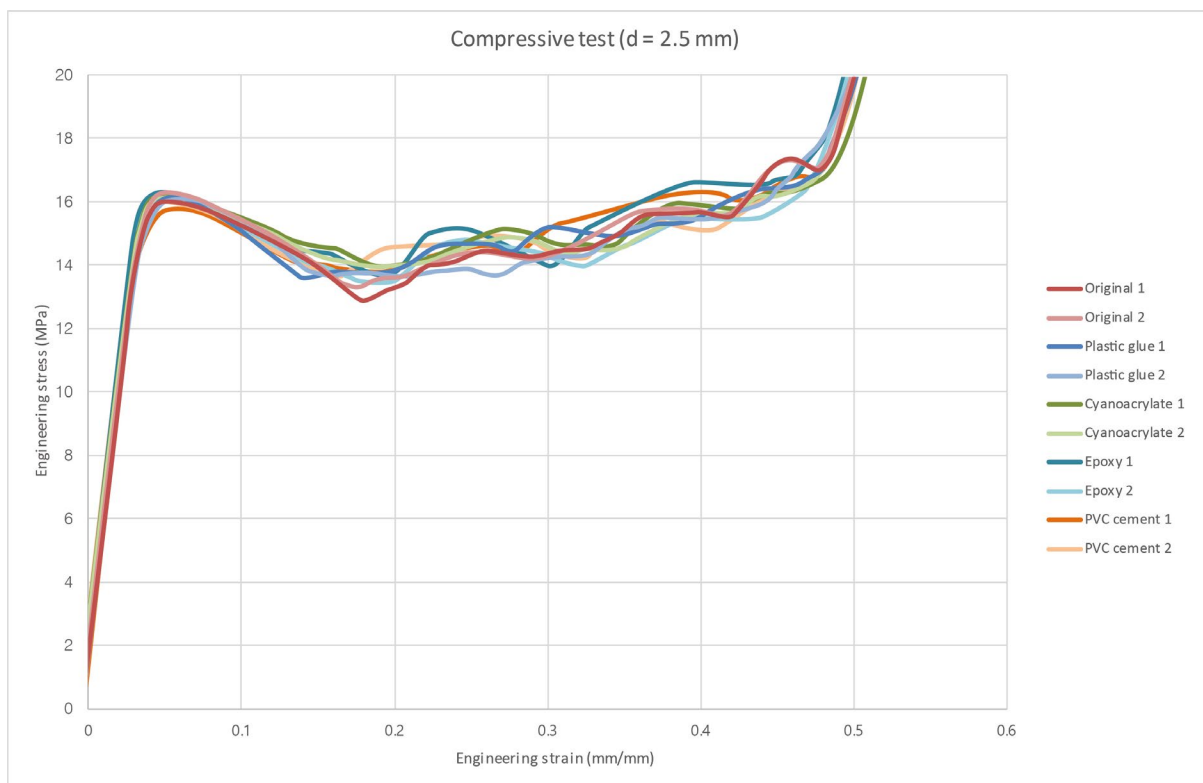
(a)
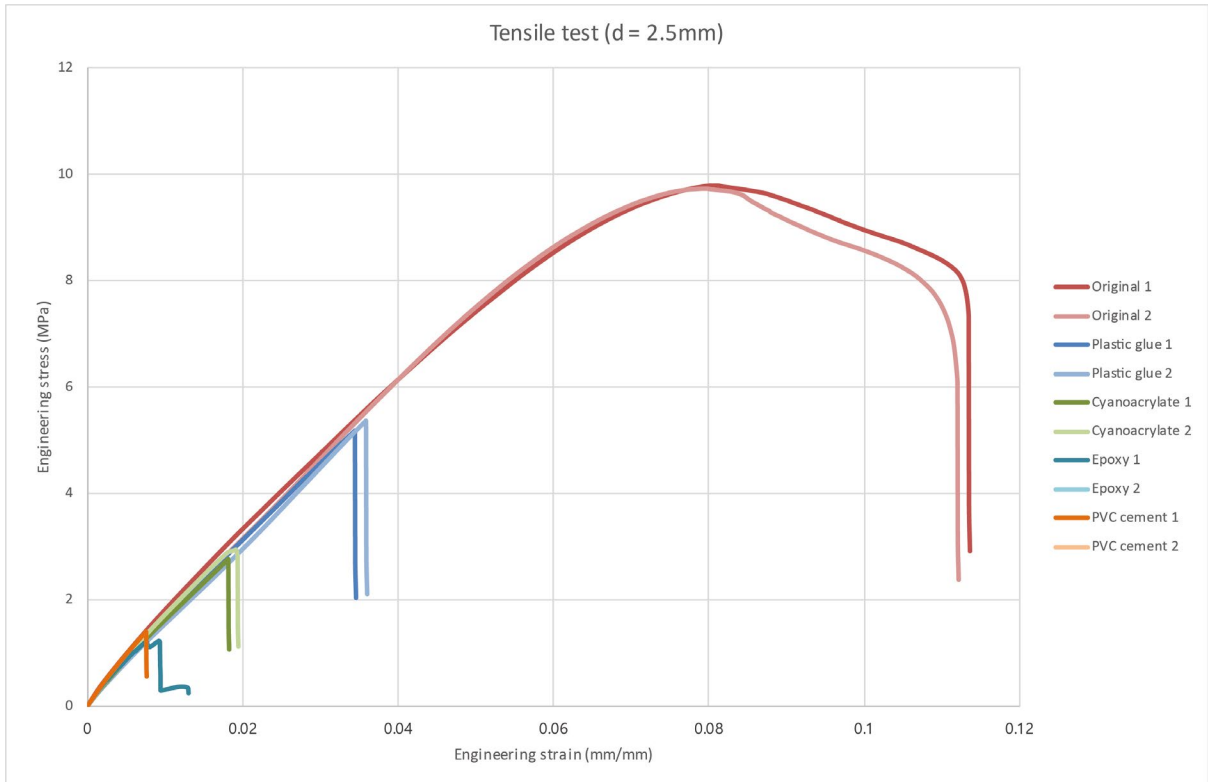
(b)
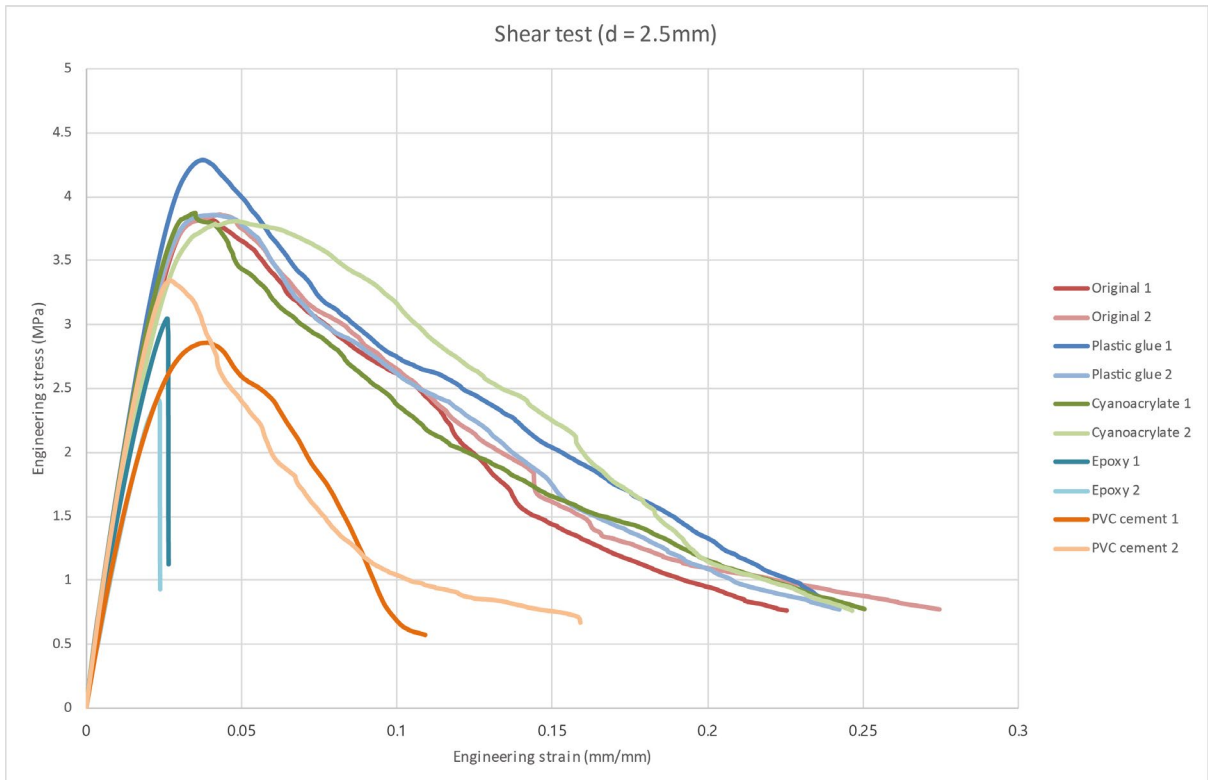
(c)

Fig B1 Engineering stress-strain curve extracted from tests; (a) compression, (b) tensile, and (c) shear test. The plastic adhesives showed the most similar mechanical behavior to the original specimen as well as appearance among them.

Appendix C

Specificaion of the specimen

Lists of specification of the standard and joined specimens used in four different tests. In the specimen label, the first letter 'C', 'T', 'S', and 'B' represent 'compressive', 'tensile', 'shear' and 'three-point bending' test, while the second letter 'S' and 'J' represent 'standard' and 'joined' specimen, respectively. For the tensile and shear test, only the lattice structure part of the sample is included, making the same bonding surface area depending on the strut diameter.

Specimen label	Strut diameter (mm)	Quantity	Designed dimension				Volume (mm3)	Bonding surface area (mm2)
			Length (mm)	Width (mm)	Height (mm)	Mass (g)		
C-S-10	1.0	6	20	20	40	2.18	1821.69	105.14
C-S-15	1.5	6	20	20	40	4.81	3755.43	151.70
C-S-20	2.0	6	20	20	40	7.53	6056.65	194.27
C-S-25	2.5	6	20	20	40	10.65	8499.69	232.84
C-J-10	1.0	6	20	20	40	2.18	1821.69	105.14
C-J-15	1.5	6	20	20	40	4.81	3755.43	151.70
C-J-20	2.0	6	20	20	40	7.53	6056.65	194.27
C-J-25	2.5	6	20	20	40	10.65	8499.69	232.84
T-S-10	1.0	6	40	20	20	2.18	1821.69	105.14
T-S-15	1.5	6	40	20	20	4.81	3755.43	151.70
T-S-20	2.0	6	40	20	20	7.53	6056.65	194.27
T-S-25	2.5	6	40	20	20	10.65	8499.69	232.84
T-J-10	1.0	6	40	20	20	2.18	1821.69	105.14
T-J-15-	1.5	6	40	20	20	4.81	3755.43	151.70
T-J-20-	2.0	6	40	20	20	7.53	6056.65	194.27
T-J-25	2.5	6	40	20	20	10.65	8499.69	232.84
S-S-10	1.0	6	20	40	20	2.18	1821.69	105.14
S-S-15	1.5	6	20	40	20	4.81	3755.43	151.70
S-S-20	2.0	6	20	40	20	7.53	6056.65	194.27
S-S-25	2.5	6	20	40	20	10.65	8499.69	232.84
S-J-10	1.0	6	20	40	20	2.18	1821.69	105.14
S-J-15	1.5	6	20	40	20	4.81	3755.43	151.70
S-J-20	2.0	6	20	40	20	7.53	6056.65	194.27
S-J-25	2.5	6	20	40	20	10.65	8499.69	232.84
B-S-10	1.0	6	60	20	20	3.27	2732.54	105.14
B-S-15	1.5	6	60	20	20	7.21	5633.18	151.70
B-S-20	2.0	6	60	20	20	11.32	9084.96	194.27
B-S-25	2.5	6	60	20	20	15.98	1.275E+04	232.84
B-J-10	1.0	6	60	20	20	3.27	2732.54	105.14
B-J-15	1.5	6	60	20	20	7.21	5633.18	151.70
B-J-20	2.0	6	60	20	20	11.32	9084.96	194.27
B-J-25	2.5	6	60	20	20	15.98	1.275E+04	232.84

Appendix D

Table C1

Average of six specimens in each compression test with standard deviation

Specimen	Strut diameter (mm)	Compressive modulus (MPa)	Yield strength (MPa)
Standard	1.0	40.59 ± 0.42	1.23 ± 0.01
	1.5	121.57 ± 0.68	4.14 ± 0.09
	2.0	253.93 ± 2.77	7.72 ± 0.11
	2.5	431.52 ± 3.03	13.70 ± 0.19
Joined	1.0	38.45 ± 0.69	1.07 ± 0.05
	1.5	116.08 ± 1.76	4.10 ± 0.07
	2.0	245.87 ± 2.11	7.55 ± 0.09
	2.5	426.32 ± 3.35	13.69 ± 0.14

Table C2

Average of six specimens in each tensile test with standard deviation

Specimen	Strut diameter (mm)	Tensile modulus (MPa)	Yield strength (MPa)
Standard	1.0	35.39 ± 1.16	0.66 ± 0.05
	1.5	89.92 ± 3.78	3.12 ± 0.06
	2.0	124.59 ± 5.23	5.39 ± 0.17
	2.5	154.30 ± 4.51	9.08 ± 0.27
Joined	1.0	31.65 ± 1.93	0.41 ± 0.07
	1.5	83.04 ± 5.56	0.92 ± 0.39
	2.0	140.98 ± 4.46	1.48 ± 0.42
	2.5	160.18 ± 8.14	4.67 ± 0.49

Table C3

Average of six specimens in each shear test with standard deviation

Specimen	Strut diameter (mm)	Shear modulus (MPa)	Yield strength (MPa)
Standard	1.0	26.20 ± 1.08	0.35 ± 0.01
	1.5	87.98 ± 11.01	1.26 ± 0.13
	2.0	121.14 ± 3.98	2.29 ± 0.13
	2.5	142.62 ± 12.22	4.18 ± 0.18
Joined	1.0	26.73 ± 1.22	0.34 ± 0.02
	1.5	85.51 ± 8.15	1.19 ± 0.16
	2.0	112.95 ± 3.20	2.28 ± 0.18
	2.5	145.09 ± 17.23	4.15 ± 0.10

Table C4

Average of six specimens in each three-point bending test with standard deviation

Specimen	Strut diameter (mm)	Flexural modulus (MPa)	Yield strength (MPa)
Standard	1.0	17.46 ± 0.74	0.27 ± 0.01
	1.5	54.71 ± 1.30	0.92 ± 0.02
	2.0	121.90 ± 2.35	2.30 ± 0.20
	2.5	211.45 ± 2.36	4.13 ± 0.15
Joined	1.0	13.14 ± 1.54	0.21 ± 0.06
	1.5	36.90 ± 10.60	0.54 ± 0.25
	2.0	105.42 ± 6.33	1.27 ± 0.38
	2.5	201.36 ± 6.16	2.52 ± 0.55

References

1.   Bakker C, den Hollander M, Peck D, Balkenende AJCM. Circular Product Design: Addressing Critical Materials through Design. 2019.

2.   Den Hollander MC, Bakker CA, Hultink EJJJoIE. Product design in a circular economy: Development of a typology of key concepts and terms. 2017;21(3):517-25.

3.   MacArthur EJJoIE. Towards the circular economy. 2013;2:23-44.

4.   Giurco D, Littleboy A, Boyle T, Fyfe J, White SJR. Circular economy: questions for responsible minerals, additive manufacturing and recycling of metals. 2014;3(2):432-53.

5.   Korhonen J, Honkasalo A, Seppälä JJEe. Circular economy: the concept and its limitations. 2018;143:37-46.

6.   Mihelcic JR, Crittenden JC, Small MJ, Shonnard DR, Hokanson DR, Zhang Q, et al. Sustainability science and engineering: the emergence of a new metadiscipline. 2003;37(23):5314-24.

7.   Vayre B, Vignat F, Villeneuve FJPC. Designing for additive manufacturing. 2012;3:632-7.

8.   Manfredi D, Ambrosio E, Calignano F, Krishnan M, Canali R, Biamino S, et al. Direct metal laser sintering: an additive manufacturing technology ready to produce lightweight structural parts for robotic applications. 2013.

9.   Nguyen DSJJoAMD, Systems,, Manufacturing. Design of lattice structure for additive manufacturing in CAD environment. 2019;13(3):JAMDSM0057-JAMDSM.

10.   Green JA. Aluminum recycling and processing for energy conservation and sustainability: ASM International; 2007.

11.   Giurco D, Stewart M, Suljada T, Petrie JJPottaeere, Noosa, Australia. Copper recycling alternatives: an environmental analysis. 2006:20-3.

12.   Maga D, Hiebel M, Thonemann NJR, Conservation, Recycling. Life cycle assessment of recycling options for polylactic acid. 2019;149:86-96.

13.   Chu C, Graf G, Rosen DWJC-AD, Applications. Design for additive manufacturing of cellular structures. 2008;5(5):686-96.

14.   Tao W, Leu MC, editors. Design of lattice structure for additive manufacturing. 2016 International Symposium on Flexible Automation (ISFA); 2016: IEEE.

15.   Beyer CJJoMS, Engineering. Strategic implications of current trends in additive manufacturing. 2014;136(6).

16.   Azman AH. Method for integration of lattice structures in design for additive manufacturing 2017.

17.   Pelanconi M, Barbato M, Zavattoni S, Vignoles G, Ortona AJM, Design. Thermal design, optimization and additive manufacturing of ceramic regular structures to maximize the radiative heat transfer. 2019;163:107539.

18.   Nguyen DS, Tran TT, Le DK, Le VT, editors. Creation of Lattice Structures for Additive Manufacturing in CAD Environment. 2018 IEEE International Conference on Industrial Engineering and Engineering Management (IEEM); 2018: IEEE.

19.   Tamburrino F, Graziosi S, Bordegoni MJJoC, Engineering ISi. The design process of additively manufactured mesoscale lattice structures: a review. 2018;18(4).

20.   Hao L, Raymont D, Yan C, Hussein A, Young P, editors. Design and additive manufacturing of cellular lattice structures. The International Conference on Advanced Research in Virtual and Rapid Prototyping (VRAP) Taylor & Francis Group, Leiria; 2011.

21.   Nguyen J, Park S-I, Rosen DW, Folgar L, Williams J, editors. Conformal lattice structure design and fabrication. Solid Freeform Fabrication Symposium, Austin, TX; 2012.

22.   Wang Y, Jing S, Liu Y, Song G, Qie L, Xing HJAiME. Generative design method for lattice structure with hollow struts of variable wall thickness. 2018;10(3):1687814017752482.

23.   Gibson I, Rosen DW, Stucker B. Additive manufacturing technologies: Springer; 2014.

24.   Saboori A, Aversa A, Marchese G, Biamino S, Lombardi M, Fino PJAS. Application of directed energy deposition-based additive manufacturing in repair. 2019;9(16):3316.

25.   Jenett B, Cellucci D, Gregg C, Cheung K, editors. Meso-scale digital materials: modular, reconfigurable, lattice-based structures. ASME 2016 11th International Manufacturing Science and Engineering Conference; 2016: American Society of Mechanical Engineers Digital Collection.

26.   Xu Z, McCann C, Dollar AM, editors. Design of a Reconfigurable Modular Chain for Folding 3D Lattice Structures. ASME 2016 International Design Engineering Technical Conferences and Computers and Information in Engineering Conference; 2016: American Society of Mechanical Engineers Digital Collection.

27.   Cheung KC, Gershenfeld NJs. Reversibly assembled cellular composite materials. 2013;341(6151):1219-21.

28.   Jenett B, Calisch S, Cellucci D, Cramer N, Gershenfeld N, Swei S, et al. Digital morphing wing: active wing shaping concept using composite lattice-based cellular structures. 2017;4(1):33-48.

29.   Dong L, Wadley HJCS, Technology. Mechanical properties of carbon fiber composite octet-truss lattice structures. 2015;119:26-33.

30.   Ashby MF, Evans T, Fleck NA, Hutchinson J, Wadley H, Gibson L. Metal foams: a design guide: Elsevier; 2000.

31.   Nowacki J, Krajewski S, Grabian JJWTR. Problems of aluminum foam soldering. 2014;86(1).

32.   Wegman RF, Tullos TR. Handbook of adhesive bonded structural repair: William Andrew; 1992.

33.   Biffi CA, Colombo D, Previtali B, Tuissi A, editors. Fiber laser welding of copper based open cell foams. 9th CIRP International Conference on Intelligent Computation in Manufacturing Engineering, CIRP ICME 2014; 2014: Elsevier.

34.   Bakker C, Poppelaars RBFJDftce. 14 Design for product integrity in a Circular Economy. 2018.

35.   Graf GC, Chu J, Engelbrecht S, Rosen DW, editors. Synthesis methods for lightweight lattice structures. ASME 2009 International Design Engineering Technical Conferences and Computers and Information in Engineering Conference; 2009: American Society of Mechanical Engineers Digital

Collection.

36.   Ashby MJPTotRSAM, Physical, Sciences E. The properties of foams and lattices. 2006;364(1838):15-30.

37.   Ling C, Cernicchi A, Gilchrist MD, Cardiff PJM, Design. Mechanical behaviour of additively-manufactured polymeric octet-truss lattice structures under quasi-static and dynamic compressive loading. 2019;162:106-18.

38.   Deshpande VS, Fleck NA, Ashby MFJJotM, Solids Po. Effective properties of the octet-truss lattice material. 2001;49(8):1747-69.

39.   Tancogne-Dejean T, Spierings AB, Mohr DJAM. Additively-manufactured metallic micro-lattice materials for high specific energy absorption under static and dynamic loading. 2016;116:14-28.

40.   Corporation H. The Loctite Design Guide for Bonding Plastics. 2011;6.

41.   ASTM D1621-16, Standard Test Method for Compressive Properties of Rigid Cellular Plastics, ASTM International, West Conshohocken, PA,. 2016.

42.   Park S-I, Rosen DW, Choi S-k, Duty CEJAM. Effective mechanical properties of lattice material fabricated by material extrusion additive manufacturing. 2014;1:12-23.

43.   Gorguluarslan RM, Park S-I, Rosen DW, Choi S-KJJoMD. A multilevel upscaling method for material characterization of additively manufactured part under uncertainties. 2015;137(11).

44.   ASTM D2095-96, Standard Test Method for Tensile Strength of Adhesives by Means of Bar and Rod Specimens, ASTM International, West Conshohocken, PA. 2015.

45.   ASTM D5656, Standard Test Method for Thick-Adherend Metal Lap-Shear Joints for Determination of the Stress-Strain Behavior of Adhesives in Shear by Tension Loading, ASTM International, West Conshohocken, PA. 2010.

46.   ISO 11003-2:2019, Adhesives - Determination of shear behaviour of structural adhesives - Part 2: Tensile test method using thick adherends. 2019.

47.   O'Masta MR, Dong L, St-Pierre L, Wadley H, Deshpande VSJJotM, Solids Po. The fracture toughness of octet-truss lattices. 2017;98:271-89.

48.   ASTM D790-10, Standard Test Methods for Flexural Properties of Unreinforced and Reinforced Plastics and Electrical Insulating Materials, ASTM International, West Conshohocken, PA. 2010.

49.   Xu Y, Zhang H, Šavija B, Figueiredo SC, Schlangen EJM, Design. Deformation and fracture of 3D printed disordered lattice materials: Experiments and modeling. 2019;162:143-53.

50.   FEPA-Standard 42-2. 2006.

51.   Uehara K, Sakurai MJJoMPT. Bonding strength of adhesives and surface roughness of joined parts. 2002;127(2):178-81.

52.   Ghumatkar A, Budhe S, Sekhar R, Banea M, Barros SdJLAJoS, Structures. Influence of adherend surface roughness on the adhesive bond strength. 2016;13(13):2356-70.

53.   Woo SJSSd. Reliability Design of Mechanical Systems. 2017;10:978-3.

54.   Horn TJ, Harrysson OLJSp. Overview of current additive manufacturing technologies and selected applications. 2012;95(3):255-82.

55.	Piemonte V, Sabatini S, Gironi FJJoP, Environment t. Chemical recycling of PLA: a great opportunity towards the sustainable development? 2013;21(3):640-7.

56.	Maskery I, Hussey A, Panesar A, Aremu A, Tuck C, Ashcroft I, et al. An investigation into reinforced and functionally graded lattice structures. 2017;53(2):151-65.

57.	Brennan-Craddock J, Brackett D, Wildman R, Hague R, editors. The design of impact absorbing structures for additive manufacture. Journal of Physics-Conference Series; 2012.

58.	Fleck NA, Deshpande VS, Ashby MFJPotRSAM, Physical, Sciences E. Micro-architectured materials: past, present and future. 2010;466(2121):2495-516.

59.	Silva LF. Design rules and methods to improve joint strength. Handbook of adhesion technology2011.

60.	Ebnesajjad S, Landrock AH. Adhesives technology handbook: William Andrew; 2014.

61.	Austermann J, Redmann AJ, Dahmen V, Quintanilla AL, Mecham SJ, Osswald TAJJoCS. Fiber-Reinforced Composite Sandwich Structures by Co-Curing with Additive Manufactured Epoxy Lattices. 2019;3(2):53.